UNIVERSITY OF CENTRAL OKLAHOMA

GRADUATE COLLEGE

3D PRINTED OBJECT TOPOGRAPHY ANALYSIS AND THE VIABILITY FOR FORENSIC EXAMINATION

A THESIS

SUBMITTED TO THE GRADUATE FACULTY

In partial fulfillment of the requirements for the

Degree of

MASTER OF FORENSIC SCIENCE

By

COOPER BLAIR

Edmond, Oklahoma

2025

3D PRINTED OBJECT TOPOGRAPHY ANALYSIS AND THE VIABILITY FOR FORENSIC EXAMINATION

A THESIS APPROVED FOR THE

W. ROGER WEBB FORENSIC SCIENCE INSTITUTE

By ______________________

Eric Law, Ph.D. Committee Chairperson

____

James Creecy, Ph.D. Committee Member

____

Kirk Garrison, B.S. Committee Member

Dedicated to my beloved wife, whose unwavering support and encouragement have been my greatest strength.

Acknowledgements

I would like to sincerely thank Dr. Eric Law for his steadfast support, guidance, and invaluable contributions to this project. I would also like to extend my gratitude to Dr. James Creecy and Kirk Garrison for their thoughtful feedback and assistance throughout the process of this research.

Table of Contents

List of Figures

Abstract

With the recent surge of advanced commercially available 3D printing technologies, individuals have the ability to create virtually untraceable firearm components from the comfort of their home. As these untraceable firearms are becoming more popular, there is a need to determine viable methods of source identification of these 3D printed objects. Both the printer hot end nozzle and print bed surfaces leave distinct characteristics that are observable upon the surfaces of the 3D printed objects. It is hypothesized that the thermoplasticity of the polymers used for printing inherits the characteristics present on the print bed surface and microscopic characteristics of the hot end nozzles used to print the objects. There have been few studies on the topic of the forensic analysis of 3D printer related evidence, and fewer that use advanced algorithms to objectively determine the similarity of 3D printed evidence. The goal of this research was to determine whether toolmarks found on 3D printed objects are distinct enough to identify or exclude a 3D printed object as originating from a specific source. To test this, 150 printed objects were created with ten different print beds and ten different nozzles, with 15 prints for each bed-nozzle pair. 3D scans of the top and bottom surfaces of each object were made using the Cadre Forensics TopMatch-GS system. Cadre's pattern-matching algorithms were then applied to the 3D scans, which gave each comparison a score between 0 and 1.0 depending on how similar the surfaces are. All bottom and top layer scans were intercompared, resulting in a total of 11,175 comparisons for each top and bottom surface. The data was analyzed using receiver operating characteristic (ROC) curves and area under curve (AUC) scores. AUC scores demonstrated that the algorithm was able to consistently and correctly differentiate between same and different source printed objects. This study demonstrates that source identification of 3D printed objects using toolmarks may be viable for forensic examination.

Introduction

In the field of forensic firearm examination, examiners are tasked with the comparison of fired cartridge cases and bullets at a crime scene to cartridge cases and bullets test fired from a suspect's firearm. Characteristics created on the firearm's mechanical structures during the manufacturing process are reproduced onto cartridge cases and bullets expended from the firearm. This process allows firearm examiners to make conclusions about the source of the fired cartridge cases from the crime scene. If a firearm is found on the scene of a crime, an investigator can utilize the serial number embedded in the receiver of the firearm to determine previous owners of the firearm. The Gun Control Act of 1968 mandated that all non-antique firearms must have a unique identifier on the receiver of the firearm (Vizzard, 1999). With this, criminals have been obliterating serial numbers on firearms for decades. However, the recent surge in additive manufacturing (3D printing) technology has enabled these criminals to simply create the receivers of (or entire) firearms without any unique identifiers. These firearms are referred to as "ghost guns" and have no means of identifying where they originated from.

In 2013, Cody Wilson of "Defense Distributed" created a design for a firearm made of almost completely 3D printed parts and dubbed it "The Liberator". Many tests have been conducted assessing the Liberator's destructive potential, reliability, and ease of assembly. Much like standard firearm manufacturing, the theory of characteristics created on a firearm during the manufacturing process extends to the 3D printing of firearms. Recent developments in research have shown that microscopic examination of the print bed surface, printer hot end nozzle, and the topographical signatures of the 3D printed object may be able to link 3D printed objects to a specific 3D printer or another 3D printed object from the same source. However, studies conducted by Pavlovich and Garrison (2023) and Aronson et al. (2021) are limited in scope and have not taken advantage of algorithm-assisted comparison to quantitatively determine how similar 3D printed topographical signatures are. It is hypothesized that the topographical signatures found within 3D printed objects can be a reliable source of identification between 3D printed objects and the 3D printers from which they originated. In order to understand how these topographical signatures are made, it is important to understand the process of 3D printing and various additive manufacturing techniques.

History & Overview of 3D Printing

Additive manufacturing is a technique that deposits thin layers of material onto itself to create a complex three-dimensional object. Items are more commonly manufactured through the process of subtractive manufacturing. This is where an object is created by the subsequent removal of materials using cutting tools, such as milling. Additive manufacturing has become increasingly popular due to the advancement of 3D printing technology. 3D printers utilize several different materials and additive manufacturing techniques to create complex structures from 3D modeled files. 3D printing techniques have been used to construct houses, create fast prototypes for engineering, and even build biomedical devices (Ngo et al., 2018). Although 3D printing is a novel method of manufacturing, it has been around for over three decades.

The earliest 3D printing technique, called stereolithography (SLA), was developed by Charles Hull in 1986 (Su & Al'Aref, 2018). SLA applies a UV light beam to a layer of resin or monomer solution. This creates a chain reaction that hardens the selected material. Excess material becomes a supportive structure to hold subsequent layers of material. Once printing is completed, the excess material is removed from the object (Ngo et al., 2018). This early method of manufacturing sparked the advancement of additive manufacturing processes and the technology that is seen today. As technology advances, 3D printers are becoming commercially available and consumer friendly. These commercially available printers are becoming very popular with individuals all over the world. These consumer-friendly 3D printers commonly use an additive manufacturing technique known as fused deposition modeling (FDM).

In FDM, spooled filaments in the form of thermoplastic polymers are extruded through a heated nozzle. As the filament extrudes through the heated nozzle, it reaches a semi-liquid state. The thermoplasticity of the filament allows it to bind itself to previous layers of material and harden at room temperature (Ngo et al., 2018). This extrusion assembly is mounted to a machine that moves along the x, y, and z axes and is controlled by a complex computerized system (Figure 1). FDM 3D printers are becoming more common due to the low cost of materials, low

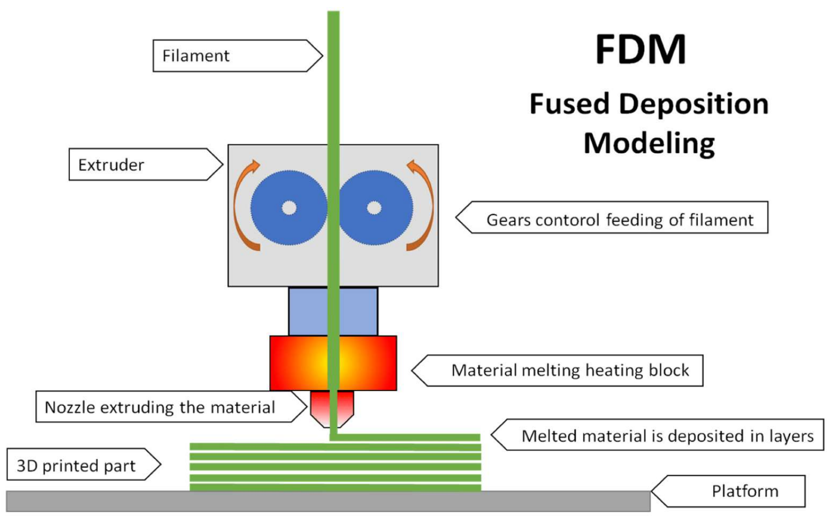

Figure 1. A diagram depicting the FDM 3D printing process technique (Przekop, R. E. et al.).

waste of materials, ease of access, and ease of use. Once purchased, these 3D printers typically come assembled and preloaded with the programs necessary to begin the 3D printing process. Various 3D models can be downloaded from websites for free or can be custom made using a 3D modeling program. Once the model is finished, the 3D model is run through a program called a “slicer”. This program slices the 3D model into several small layers that the 3D printer translates into layers it will print when the process begins. As the popularity of commercially available additive manufacturing technology rises, so do its applications for illicit activities. 3D printing firearm components has become a popular hobby for both civilians and criminals, but this interest is creating legal issues at the federal level.

History of Serial Numbers

The Gun Control Act of 1968 is a detailed policy that created the legal mainframe for national gun policies in the United States (Vizzard, 1999). One of the most notable reforms was a mandated addition of unique serial identifiers on the receiver (or frame) of every non-antique firearm. The receiver is the only part of the firearm required to have a serial identifier. This is due to the receiver being the most vital part of the firearm. Consequently, only the receiver of the firearm is legally considered a "firearm" and must be regulated. With this, all other components of firearms are not required to have serial numbers and can be purchased without a background check. These serial identifiers are permanently embedded into the receiver of every firearm using different manufacturing techniques. The serial identifiers are linked to information regarding the state, city, and name of the firearm manufacturer. Detailed records are kept as to who bought a firearm and the serial number associated with that firearm. If a firearm is found at the scene of a crime, the purchase history of the firearm can be traced back to the most recent owner of the firearm because of the serial identifier.

Serial number tracing is not always effective, as private, and undocumented sales of firearms between individuals is perfectly legal and very common. However, this tracing strategy is still used to generate leads. As criminals became aware of serial number tracing, it became popular to obliterate serial numbers from the receiver of firearms used for illicit activities. Forensic firearm serial number restoration techniques were utilized to identify firearms with obliterated serial numbers (Heard, 2008). Although this method is effective, the advancement of 3D printing technology is creating more modern issues.

Since 3D printed objects come from custom 3D modeled files, the design of the object is under the control of the individual printing the object. The use of a 3D printer to create the receiver of a firearm removes the necessity of a traceable serial number attached to the firearm. Since other parts of the firearms are neither regulated nor branded with serial numbers, this creates the possibility of firearms that are virtually untraceable. As these untraceable firearms become more common, the law attempts to keep up with the legal ramifications and loopholes these firearms produce.

Legal Aspects of Privately Manufactured Firearms

Currently, no federal laws prohibit the private manufacturing of firearms for personal use in the United States. As long as the firearm is created without the intent to be sold or distributed, the firearm is considered legal, even without a serial number. Since the receivers of most modern handguns are made from polymers, 3D printed receivers pose a small threat to the structural integrity of the firearm. Although handguns can do devastating amounts of damage, semi-automatic rifles have larger magazine sizes, more powerful ammunition, and have a longer range than handguns. AR-15 semi-automatic rifles are becoming an increasing concern worldwide because of their use in shooting incidents and acts of terror. Similar to handguns, receivers are the only part of an AR-15 style rifle that is legally considered a firearm. These receivers are commonly made from high-grade aluminum and are precisely machined to fit the other components of the rifle. The AR-15 receiver requires extensive gunsmithing knowledge and specialty tools to create by hand, but legal loopholes and new machinery are making them easier to create and more accessible than ever.

As mentioned, receivers are the only regulated part of a firearm and cannot be purchased online without a background check. This has sparked debate regarding when a piece of aluminum, steel, or plastic legally becomes a lower receiver. This discussion led to the creation of the “80 Percent” lower receiver. Manufacturers have been creating and selling unfinished lower receivers without serial numbers or background checks. This is because 80 percent of a lower receiver can legally be completed without meeting the Gun Control Act (GCA) definition of a firearm. This enables individuals with little machining experience to create fully functional AR-15 lower receivers in the comfort of their garage workshop. This process only becomes easier with the utilization of guides, jigs, and even machines to do the milling for you, such as Defense Distributed’s “Ghost Gunner” (Greenberg, 2014). The Ghost Gunner is a small desktop milling machine designed to finish milling 80 percent lower receivers. Once an individual is in possession of the Ghost Gunner and an 80 percent lower receiver, all that is needed is to put the unfinished receiver into the machine, turn it on, and set the system to run the lower receiver operation. This process requires no previous experience, and once it is finished, an untraceable, high-quality aluminum AR-15 lower receiver is ready for use. Although the thought of completely untraceable firearms is daunting, forensic firearm examiners have developed and utilized many other techniques to determine the origins of firearms and firearm evidence.

Forensic Analysis of Firearm Evidence

In 1906, riots broke out in Brownsville, Texas, where members of the US infantry opened fire on the rioters. As a result, staff at the Frankfort Arsenal were asked to identify which weapons were fired by the 25th Infantry during the massacre. The staff used magnified photos of the firing pin impressions on the primer of expended cartridge cases with pattern comparison techniques to positively identify which firearms were used in the shooting (Heard, 2008). In

1912, Victor Balthazard took photomicrographs of bullet lands and grooves to attempt to identify the model of firearm from which a bullet originated. From his examination, he noticed that the tools used in cutting the rifling of the barrel never leave the exact same markings. These distinct markings are then imparted onto the bullet as it passes through the barrel. Balthazard theorized that it was possible to link a fired bullet to the specific barrel it originated from. With the theory of unique markings present in every firearm barrel, Balthazard extended his work to other parts of the firearm.

Balthazard began observing unique striations present within interactions caused by the firing pin, breech face, ejector, and extractor. Balthazard extended his theory to include these firearm interactions, reasoning that every interaction with a tool produces unique markings that are imparted onto surfaces they come into contact with (Heard, 2008). Taking photomicrographs of bullets and spent cartridge cases was time consuming and laborious, so in 1925 comparison microscopy was utilized in the comparison of firearm evidence. Comparison microscopes allow examiners to view two magnified images of spent cartridge cases or fired bullets simultaneously. This technological advancement made comparing firearm evidence clearer and more reliable than ever before. As more techniques and technology were utilized by firearm examiners, some in the scientific community began critiquing the methodologies behind firearm evidence identifications and exclusions.

Unlike DNA evidence, conclusions drawn from firearm evidence are based solely on the observations and opinion of the examiner. The Association of Firearm and Toolmark Examiners (AFTE) theory of identification is founded on scientific principles, but ultimately subjective in nature. This means that the quality and reliability of conclusions drawn from analysis are the professional opinion of the firearm examiner. This is because the theory of identification as it pertains to firearm and toolmark evidence is based on "sufficient agreement" of toolmarks (AFTE, 1985). Sufficient agreement is a term that relates to the significant duplication of random toolmarks and patterns imparted onto a surface. According to the AFTE Theory of Identification, agreement is significant when the agreement in individual characteristics exceeds the best agreement demonstrated between toolmarks known to have been produced by different tools and is consistent with agreement demonstrated by toolmarks known to have been produced by the same tool (AFTE, 1985). Agreement and conclusions are drawn using class, subclass, and individual characteristics.

Class characteristics are features determined before the manufacturing process and are used to provide general insight into the make and model of the firearm (Mattijssen, 2020). Examples of class characteristics are caliber, breech face pattern, and number of rifling lands and grooves. Class characteristics are often used in the elimination of firearms evidence when a test fired cartridge or bullet is compared to the original evidence. Class characteristics cannot be used to make an identification because they are not unique to a specific firearm. Subclass characteristics are discernible features of an object that are present on consecutively manufactured items by a tool in a specific state of wear (Mattijssen, 2020). Subclass characteristics are a subset of class characteristics and often look similar to individual characteristics when observed using comparison microscopy. However, subclass characteristics are often observed on consecutively manufactured tools. This makes subclass characteristics not suitable for identification purposes due to their repeatability. Examiners must be aware of the existence of subclass characteristics and familiar with the manufacturing methods that increase the likelihood of subclass characteristics present within the firearm. Individual characteristics are markings imparted on firearm evidence that are specific to a single firearm. These characteristics are randomly imparted on the firearm during the manufacturing process. The state of wear and conditions that the firearm is exposed to are also contributing factors of individual characteristics. Using these characteristics can greatly assist examiners in drawing conclusions about firearm evidence. AFTE defines four different conclusions that can be drawn from firearm evidence (AFTE, 1992).

1. Identification

   Identifications are reached when an examiner has observed a sufficient amount of agreement between the markings present on two items of firearms evidence.

2. Inconclusive

   a. A conclusion drawn when two pieces of evidence share class characteristics and some individual characteristics, but are insufficient for an identification.

   b. A conclusion drawn when two pieces of evidence share class characteristics, but there is not enough sufficient agreement or disagreement to determine any other conclusions.

   c. A conclusion drawn when two pieces of evidence share class characteristics and have disagreement of individual characteristics, but insufficient for an elimination.

3. Elimination

   Eliminations occur when there is a significant disagreement of class characteristics or individual characteristics between items of firearm evidence.

4. Unsuitable

   Items such as deformed or fragmented bullets can be considered unsuitable for examination if there are no discernible characteristics present on the evidence.

Inconclusive conclusions have been under scrutiny from many due to the varied and non-standardized rationale utilized when making the inconclusive conclusion (Baldwin et al., 2023). However, these conclusions are necessary for consistent and comprehensive firearm and toolmark evidence analysis. Since the concern of illicit 3D printed firearm manufacturing only grows as time progresses, the need for research focused on 3D printed firearms is increasing as well. Research is currently being conducted on the structural viability and practicality of 3D printed firearms, as well as whether the same theories of uniqueness during the manufacturing process also apply to 3D printed objects.

3D Printed Firearms

3D printed firearms are becoming one of the most prevalent modern controversies. Many are not concerned because not all of the parts of the firearm can be printed at home. Some parts of the firearm must be purchased externally. It was once believed that once all the necessary parts of the firearm are present, an individual must possess a significant amount of knowledge in gunsmithing and firearm mechanisms to assemble the firearm, but that is no longer true. In 2013, Cody Wilson of Defense Distributed created a design for a firearm made out of almost completely 3D printed parts. Wilson then test-fired the 3D printed firearm and subsequently shared the files to print the firearm online. Wilson dubbed it The Liberator.

The file for the Liberator was downloaded over 100,000 times within a span of two days (Honsberger et al., 2018). At the time of its conception, there were no laws that prohibited 3D printed firearms. Even with this loophole present, the United States Department of State reached out to Wilson and demanded that he take it down (Leon, 2019). This resulted in a legal case where the United States argued that Wilson did not possess a license for selling and distributing firearms. Wilson argued that the 3D modeled files fall underneath the jurisdiction of the First

Amendment. The case concluded with the United States Department of State waiving the license requirement, allowing Wilson to distribute the files for the Liberator online freely (Leon, 2019).

The introduction of the Liberator to the world of additive manufacturing has opened many paths for future files to be used for illicit activities. As Leon's (2019) article describes, the US law presents many shortcomings in relations to laws surrounding 3D printed firearms and the distribution of dangerous files. Leon (2019) brings into question the validity of using 3D modeled files as a freedom of speech. For something to fall under the First Amendment, it must contain sufficient elements of communication. Leon (2019) then compares previous jurisdictions on tattoos falling under the First Amendment to explain why 3D modeled files also are protected by the First Amendment.

If these files are protected by the First Amendment and can continually be distributed and printed without repercussions from the government, how can law enforcement adapt? First, research must focus on the manufacturing process and assembly of the firearm itself, how viable the 3D printing process for firearm manufacturing is, and if the polymers used in the printing process can withstand the pressures a firearm emits.

An article published by Trincat et al. (2022) in the *Forensic Science International* journal focuses on the manufacturing process of a 3D printed Liberator firearm, the structural integrity of the firearm, and the processes that take place during firing. The article begins with an explanation of the printing process, the assembly process, and the test firing setup. For this experiment, four different 3D printers, representing three different 3D printing processes, were used to manufacture the firearms in this experiment (Trincat et al., 2022). The first printers were a Stratasys Fortus 250 mc (Stratasys, Ltd., USA) and a Zortrax M200 (Zortrax S.A., Poland).

Both printers utilized material extrusion (ME) techniques, which utilize the FDM manufacturing method. These printers utilized common thermoplastic filaments acrylonitrile butadiene styrene (ABS), polylactic acid (PLA), and polyethylene terephthalate glycol (PETG) to print several liberators. The third printer utilized was a Formlabs Form2 (Formlabs Inc., USA), which utilizes the VAT photopolymerization (VP) method. The VP printing method encompasses the stereolithography (SLA) printing method. This method utilized seven different selections of resins: Tough, High Temp, Grey Pro, Rigid, Flexible, and Durable, all distributed by Formlabs Inc. (Trincat et al., 2022). The fourth and final printer was the EOSINT P 395. This printer utilized the SLS printing method, a form of powder bed fusion (PBF). PBF utilizes a high-energy source to fuse powder material together, forming a three-dimensional object. Three Liberators were printed with the PA 2200 polymer sold by EOS GmbH (Trincat et al., 2022).

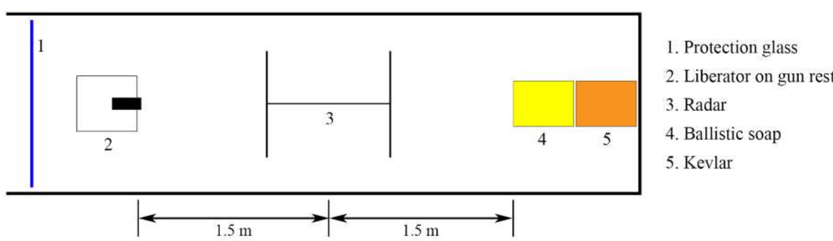

Figure 2. A diagram depicting the testing setup used in Trincat et al.'s experiment (Trincat et al., 2022).

Prior to assembling the firearms, the Liberator's pieces were closely observed and documented to highlight characteristics specific to the printing process utilized. Once carefully assembled, the firearms were put into a controlled firing chamber and fired remotely from a safe area *(Figure 2)*. Ballistics data were then collected and recorded for all successfully assembled Liberators. The least successful of the three printing methods was the firearms printed out of resin, utilizing the VP technique. Only nine of the 18 Liberators printed with VP could even be assembled, and none of them successfully discharged any rounds. This was due to the fragility of the resins used in the VP 3D printing process. The other firearms printed with the ME and PBF techniques were all assembled, and all successfully discharged rounds. Upon firing a single round, every single firearm was destroyed, and traces of the firearm were left scattered around the room and on the projectile itself.

When utilizing a mainly 3D printed firearm with the intent to harm another, this article shows that the firearm would cause a significant amount of damage to the shooter as well as the victim. This article also attests to the fragility of 3D printed materials when used as the main material for a firearm. Although the Liberator is a lethal firearm, it can only fire one round before the entire gun explodes in the shooter's hand. This property of the Liberator significantly disincentivizes the use of primarily 3D printed firearms within criminal activity. Although seeing a Liberator used on a crime scene might be very uncommon, the use of 3D printers to create components of lethal weapons and devices might be seen on more crime scenes in the future. If these firearms are used at a crime scene, the next article focuses on what types of forensic evidence investigators should expect to find.

Articles by Honsberger et al. are presented in a two-part series of an in-depth study on the Liberator 3D printed firearm. In their first article, Honsberger et al. (2018) aimed to assess the exterior ballistic properties and the wounding potential of 3D printed Liberator pistols. Honsberger et al. printed, assembled, and fired six Liberators in a controlled environment where ballistics data and traces of evidence produced by the shooting were collected. The six Liberators fired were produced using FDM printing and utilized a modified ABS filament that was intended to withstand more force than traditional ABS filament. Six Liberators were produced to fire .380 Auto ammunition. There were also three more barrels manufactured to fire .25 Auto cartridges. In order to do this, the original plans were modified to reduce the interior diameter of the barrel while keeping the outer diameter of the barrel unchanged. During the assembly process, the printed springs tended to break. Thus, only six of the nine Liberators were able to be assembled: five with the .380 Auto barrel, and one with the .25 Auto barrel.

The results of the test fires showed a large variety in the condition of the Liberators after discharging the firearm. Four out of the six Liberators had their barrels completely removed from the firearm, as well as cracked frames. The external ballistics of the Liberators also tended to be imprecise, but still produced significant wounding to the target (Honsberger et al., 2018). Honsberger et al. then discuss their findings in relation to pertinent evidence they believe would be found on the scene of a crime where a Liberator was used as a weapon. It is noted that pieces of polymer are expected to be found scattered throughout the scene of the shooting. Traces of polymers were also found on cartridge cases and even the projectiles themselves (Honsberger et al., 2018). The article then discusses the limitations of their study, emphasizing that using only the Liberator model of 3D printed firearm does not generalize at all to firearms that only contain 3D printed components. It is important to test the Liberator however, because being the first almost entirely 3D printed firearm allows it to be printed with ease. It should also be mentioned that having such a small number of Liberators printed and tested does not produce an accurate generalization of how all Liberators will function when fired. In the second part of their study, Honsberger et al. explore their observations of trace evidence more extensively.

The second article by Honsberger et al. (2019) covers the different forms of which an expelled cartridge case can take when fired by the Liberator. The experiment also goes into depth on printing the firearm for different calibers and the effects it has on the trace evidence that is produced when the firearm is fired. The article dives into the evidence found on spent cartridge cases and the bullet itself when seen under an alternate light source (ALS). When viewed under

415 nanometer wavelength illumination, the bullets and spent cartridge cases will fluoresce because of the heated chemical compounds from the 3D printed firearm during the firing process (Honsberger et al., 2019). The article then explains the different ways a shooting scene is processed when a 3D printed firearm is suspected, and the ways to collect the evidence.

This study also found that the cartridges can make an imprint on the 3D printed barrel, which can help identify the caliber of ammunition used by the 3D printed firearm. As a means of identifying the source of the fired bullet, Honsberger et al. (2019) utilized fracture matching techniques on fragments of polymers to conclude that the fragments of polymer evidence can be matched to other broken parts of the Liberator pistol. Although this conclusion might seem obvious, not much research has been previously conducted on how the heat produced by the firing process can alter the shape and structure of 3D printed polymers. This identification method applies to Liberators that have been fired and broken but does not apply to firearms that have not been fired. Recent research was conducted on different methods that can be used to identify the origins of 3D printed objects. The studies aim to match a 3D printed object to a specific 3D printer, or two 3D printed objects created from the same printer.

3D Printed Object Toolmark Analysis Methods

An exploratory study conducted by Aronson et al. (2021) applies traditional forensic tool mark analysis to 3D printed objects. The article aims to identify two objects that have been printed from the same 3D printer and if an object was printed from a specific 3D printer. Aronson et al. (2021) theorized that the plasticity of the 3D printed polymers during the printing of the base layer of an object would inherit individual characteristics present on the print bed surface. With this hypothesis in mind, Aronson et al. (2021) attempted to identify markings created on the print bed that transferred to the base of the 3D printed objects during the printing process.

Aronson et al. utilized two different FDM 3D printers, the first being a "Tevo Tarantula". The Tevo Tarantula utilized the PLA+ filament, a slightly improved version of PLA filament that is common in firearm component 3D printing. The second printer utilized was a "Flashforge Adventurer 3" that utilized PLA filament. Each of these printers employed slightly different computerized methods of printing. Along with the two different 3D printers, Aronson et al. (2021) tested two different types of 3D printing print beds for their study, a smooth glass printing bed (Tevo Tarantula) and a granular plastic printing bed (Flashforge Adventurer 3). The glass printing bed was more resistant to individualized markings, but under oblique lighting the individual markings on the glass print bed became visible. The researchers then took a forensic SIL casting of a point of interest on the print bed to compare it to the individual characteristics found on the 3D printed object. Upon microscopic examination of the 3D printed object, markings on the object consistent with markings found on the casting of the print bed were observed (Aronson et al., 2021).

Examinations of the objects printed by the Flashforge Adventurer 3 were compared to each other instead of to a print bed surface. These prints were printed on a rough print bed, which is more likely to produce a large number of granular characteristics on a printed object. Aronson et al. (2021) explained that the orientation process of the objects is critical for a sound analysis. When comparing the objects, the researcher must first determine what part of the object was used as the base for the print. Once this is done, the researcher also has to determine the start and end points of the printing process on the base layer. This is done by identifying markings made by the placement and removal of the hot end extruder from the object (Aronson et al., 2019). After the base layer is identified and the objects are correctly oriented, analysis of the object's surface can begin.

Aronson et al. (2019) discuss the difficulties and limitations of their research. Firstly, it is mentioned that there was no attempt to analyze subclass characteristics within the materials of the study. However, this was not the focus of the study, and further research into subclass characteristics within 3D printed objects was not in the scope of this study. The main difficulty of the experiment was the starting point of the print on the print bed x and y axis. Since the object only inherits markings on the base of the printed object, the area on the print bed affects the markings that would be present. For example, the base layer of an object printed at the (0in, 0in) mark on the x and y axis would have different characteristics when compared to the base layer of an object printed at the (4in, 5in) position on the print bed. This issue was explored in the analysis of the glass bed printed object, but was only discussed in the rough surface object analysis. This print location dilemma is a limiting factor in the generalizability of the research conducted. However, other research is aiming to find methods of 3D printed object identification that are not dependent on print bed location.

During the manufacturing process and regular use of tools, many different markings incidentally occur, making the tool contain characteristics unique to that tool. In their exploratory study, Pavlovich and Garrison (2023) apply the theory of unique marking during the manufacturing process to the hot end nozzle of an FDM 3D printer. The hot end nozzle of an FDM 3D printer is the last mechanism that the polymer filaments interact with before being deposited onto the print surface. Pavlovich and Garrison (2023) examined several brass nozzles and found microscopic markings incidental to manufacture present at the tips of the nozzles.

Pavlovich and Garrison (2023) reasoned that these markings may contribute to striae and other markings on the surface of a 3D printed object.

First, Pavlovich and Garrison (2023) identified areas of interest on a 3D printed object that were most likely to inherit the characteristics of the hot end nozzles. They categorized specific markings as indications of the hot end nozzle interacting with the 3D printed object. One of these markings was referred to as the “detachment point”. The detachment point is the interaction that occurs when the printer has completed a specific area of an object, removes itself from the surface of the object, and stops excess filament from extruding through the heated nozzle (Pavlovich and Garrison, 2023). This interaction was observed creating not only striae present on the printed object from the movement of the nozzle, but also a characteristic known as the “detachment tail”. The detachment tail is only produced during the detachment of the nozzle

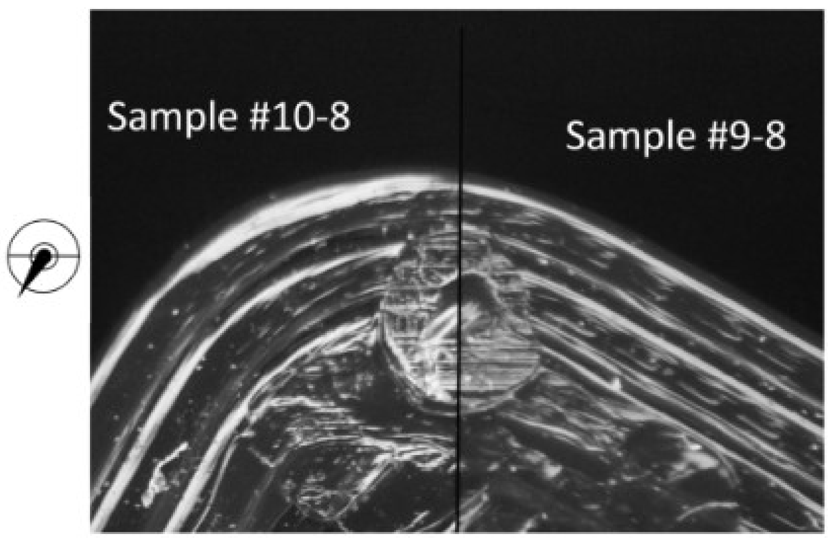

Figure 3. Matching striae of correctly oriented detachment points (Pavlovich and Garrison, 2023).

from the 3D printed object. The detachment tail and striations present within the detachment point are crucial in determining the orientation of the nozzle when the interaction occurred. Pavlovich and Garrison (2023) created a technique to correctly orient 3D printed object areas of interest when examining the object with comparison microscopy *(Figure 3)*. Pavlovich and Garrison (2023) orient the detachment tail against the direction of the striations in an axis to determine proper orientation of the examined object. When objects printed with the same hot end nozzle have their detachment points examined with comparison microscopy, consecutive matching striae are observed on the 3D printed object (Pavlovich and Garrison, 2023).

Pavlovich and Garrison's (2023) exploratory study yielded intriguing insights into the application of traditional firearm and toolmark analysis to 3D printed objects. Pavlovich and Garrison (2023) discuss the limitations of their study as well as the need for further research. Their main limitation was the lack of accounting for subclass characteristics. Since not enough significant research into 3D printing toolmarks has been conducted, it is not surprising that subclass characteristics are not accounted for within this study. The experimental analysis of subclass characteristics is simply outside the scope of Pavlovich and Garrison's (2023) research. An area that the researchers mention needs research is the implementation of pattern recognition algorithms in the toolmark analysis of 3D printed objects. Once again, conclusions made about firearm evidence are subjective in nature and are based on an examiner's personal training and experience. However, emerging technologies are creating ways to quantify the number of discernable characteristics on firearm evidence using pattern matching algorithms.

Virtual Comparison Microscopy

Virtual comparison microscopy (VCM) is an evolving technology that aims to assist in the reliability of conclusions made regarding firearms evidence. In the Interpol's most recent review of forensic firearm examinations, Mattijssen et al. (2023) cover recent literature within the field. Along with 3D printed firearms, Mattijssen et al. (2023) review proficiency testing of firearms examiners and delve into the technology of pattern matching algorithms in VCM. VCM analysis technology is creating not only high resolution 2D images of firearm evidence, but also 3D topographical images of firearm evidence. A study by Duez et al. (2018) assesses the feasibility of utilizing VCM in firearm evidence examinations. For this particular study, interest was primarily in the breech face markings on spent cartridge cases. 3D VCM differs from traditional comparison microscopy because examiners do not need the physical evidence present to conduct the analysis of firearm evidence. Traditionally, if an examiner wanted the second opinion of another examiner in another location, they would have to transport the evidence to the other examiner. With 3D VCM, a file can be sent to another examiner and analyzed virtually. This allows for digital archives of firearms evidence and data to be created, while streamlining the evidence handling workflow (Duez et al., 2018). The article describes the comparison process of the digitized evidence and the advantages it has over traditional comparison microscopy. For example, agencies with large geographic areas of service can have evidence scanned off site and then sent to a lab for analysis. This saves time and resources for the agency by eliminating transportation time and chain of custody documentation.

The instrument that Duez et al. (2018) utilized to create scans of their cartridge cases was the Cadre Forensics TopMatch-GS 3D Scanner. The TopMatch-GS utilizes photometric stereo technology and painted elastomeric gel sensor to create clear 3D topographical images without the influence of surface reflectivity. First, a cartridge case is loaded into the scanning system. Then, the painted elastomeric gel is applied to the top of the scanner using a roller. The expended cartridge cases are impressed into the elastomeric gel, and images of the gel impression are taken by a camera that utilizes imaging algorithms to create a 3D image of the cartridge's topographical surface based on the appearance of the surface under different lighting angles.

These images can then be saved in the X3P file format and are easily exported for further analysis on compatible computer systems.

Once scans of the 3 test sets (21 scans total) were acquired, Duez et al. (2018) began a large-scale validation experiment of these VCM images of expended cartridge cases. Fifteen sites and 56 participants voluntarily took part in the study. The experience of the participants varied from experts to trainees in the field of firearms examination. The study utilized several different cartridge cases fired from 9mm pistols, ranging in difficulty levels. The results of the study boast a 100% positive identification rate for examiners and a 0% false identification rate (Duez et al., 2018). This statistic does not include the trainees who participated in the study. Overall, the performance of the trained examiners utilizing VCM matches the performance of trained examiners utilizing traditional comparison microscopy. This article is one of many that aim to assess the validity of VCM systems. Some articles assess the use of pattern matching algorithms as a means of identification for forensic examiners.

In the initial study conducted on the algorithms utilized by the TopMatch-GS 3D Scanner, Weller et al. (2015) sought to evaluate the effectiveness of the instrument's automated imaging analysis algorithms. Weller et al. (2015) explain that the VCM system measures the 3D surface topography of cartridge cases and compares both the breech face impression and aperture shear marks using novel feature-based scoring algorithms. The algorithms utilize the 3D nature of the scans to compare the depth of markings between two cartridge cases. The validation study utilized 290 different firearms, over 700 cartridge cases, and underwent more than 100,000 comparisons. Weller et al. (2015) explain that the algorithms prioritize the lowest rate of false positives at the expense of having a slightly lower true positive rate. This study utilized different algorithm score thresholds, 0.5 and 0.8 out of 1.0, to determine an identification. The algorithm had a true positive rate of 99.0% when the algorithm's score threshold was calculated at a 0.5 and true positive rate of 100.0% when the algorithm's score threshold was set to a 0.8. The algorithm had a false positive rate of 0.01% when the algorithm's score threshold was calculated at a 0.5 and false positive rate of 0.0% when the algorithm's score threshold was set to a 0.8.

The study conducted by Weller et al. (2015) produced results that rival those of human examiners. Although many examiners are wary of the new technology replacing human examiners in the future, Weller et al. (2015) explain that VCM algorithms will not replace the firearms examiner, but rather be utilized as tools to assist the examiner in more effectively completing their job. Validation studies have also been conducted utilizing the algorithms as a quality control technique rather than a sole means of conclusions. A study conducted by Chapnick et al. (2020) tested a cohort of 76 qualified examiners using VCM to assist their conclusions. The overall false positive error rate was 0.43%, and the error rate for false negatives was 0.0% (Chapnick et al., 2020). Research has also been conducted comparing VCM techniques to traditional light comparison microscopy (LCM) methods.

Knowles et al. (2022) conducted a study comparing the false positive and false negative error rates of examiners when utilizing both VCM and LCM. This study also utilized scans from a Cadre Forensics TopMatch-GS 3D Scanner, as well as their 3D image analysis software. The results were very similar, with both VCM and LCM having a false positive rate of 0%. VCM had a false elimination rate of 0.39% while LCM had a false positive rate of 0.77% (Knowles et al., 2022). This not only validates the use of VCM but also implies that VCM should be used as a tool to assist examiners in making conclusions regarding firearm evidence.

Summary

Recent advances in additive manufacturing technology have created dilemmas within the field of firearms manufacturing and distribution. Due to 3D modeled files being protected by the First Amendment and their ease of access, researchers are looking for ways to identify 3D printed objects to printers and to objects printed by the same printer. Several recent techniques have surfaced with the potential to link 3D printed objects to their source, but the conclusions of these studies are subjective in nature and not easy to validate. VCM technology has provided firearms examiners with tools that assist in reaching objective conclusions of firearms evidence. However, research has not yet been conducted on 3D printed objects utilizing VCM technology to examine the viability of 3D printed evidence, as well as utilizing algorithm assisted comparison to determine levels of similarity between surfaces. The goal of this study is to explore whether 3D printed objects have the ability to be consistently traced back to the original 3D printer that printed the object. This study also seeks to determine if two different 3D printed objects can be identified as coming from the same 3D printer using characteristics of surface topographies found on the 3D printed objects.

Methodology

Illicit applications of 3D printing has become an increasing threat to law enforcement as the popularity of these technologies has increased. Along with this surge in popularity, research in the field of 3D printer forensic identification is also in great demand. Although there has been little research on the topic of 3D printer feature comparison forensics, the goal of this study was to determine the viability of toolmark comparison techniques applied to 3D printed objects. This study utilized 3D virtual comparison microscopy technology and employed algorithm assisted feature comparison software to quantitatively determine the similarity of topographical signatures present on the surfaces of 3D printed objects.

Materials

3D Printer

The Prusa MK4 printer was chosen as the instrument to print all the 3D printed objects for this study because of its reliability, ease of use, open-source nature, and high-quality prints. This printer utilized the FDM technique, where thin layers of polymer are deposited onto a print surface and subsequent layers of polymer are added onto previous layers to create a 3D object. The 3D printer was acquired solely for this study, meaning all printing and printing conditions were within a controlled environment.

Filament

The prints for this study were printed using Hatchbox PLA (Polylactic Acid) filament. PLA was chosen due to it being one of the most common and sturdy 3D printer filaments for creating firearm components. The specific branded Hatchbox PLA was chosen for its high quality and performance. The filament was stored in a plastic container along with desiccant to ensure controlled moisture levels.

3D Model

The printed object that was used for analysis was a custom file made in Autodesk Fusion 360 specifically for this study (Autodesk, 2024). The object resembled a double sided .45 Auto caliber cartridge case (*Figure 4*). The object was designed to have a flat surface at the bottom of the print and a simulated primer surface at the top of the print. The flat surface on the bottom was

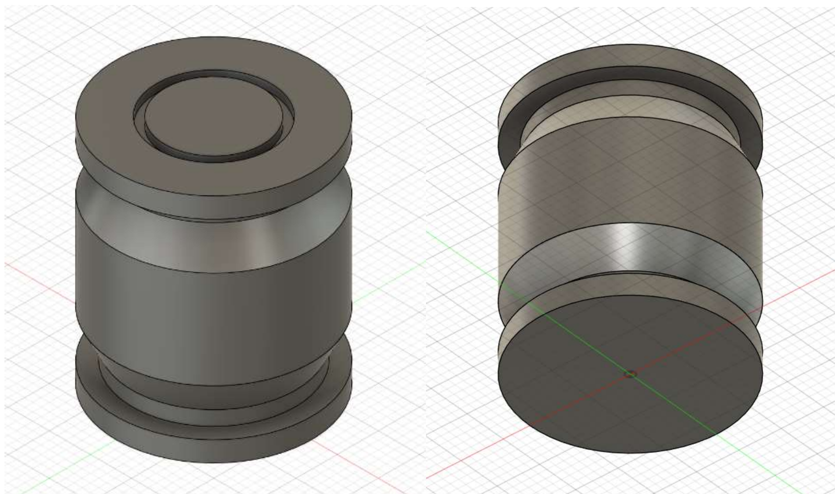

Figure 4. An image depicting the top (left) and bottom (right) of the 3D printed object used for analysis in this study.

chosen to inherit the characteristics of the print bed surface with as much surface area as possible. The simulated primer at the top of the object was chosen to inherit characteristics of the hot end nozzle surface in focus of the 3D scan. The custom .stl file was then sliced into g-code for printing using PrusaSlicer software (Prusa, 2024).

3D Printed Object Scanning & Comparison

The instrument chosen to visualize these objects was the Cadre Forensics TopMatch-GS 3D Scanner. The TopMatch-GS was designed to scan the headstamp and primer areas of cartridge cases. Thus, the design of the object used for the study resembled a .45 Auto cartridge case to be compatible with the scanner. The TopMatch-GS was chosen because of its ability to create high quality 3D images of cartridge case surface topography, as well as its ability to use powerful pattern matching algorithms to compare cartridge case topographies. The TopMatch-GS utilized photometric stereo with a painted elastomeric gel sensor to create 3D images of cartridge cases without the influence of surface reflectivity. This was important because 3D printed objects can be printed with many different types and colors of filament, which tend to reflect large amounts of light. This makes traditional comparison microscopy analysis of 3D printed evidence difficult.

The TopMatch system's algorithms are intended to assist examiners in making conclusions by determining the level of similarity between two surfaces. Two of the TopMatch system's algorithms were used for objective comparison in this study, the breech face algorithm and the aperture shear algorithm. The breech face algorithm is utilized for the impressed characteristics on the primer area of firearms evidence. Therefore, the breech face algorithm was used on the surface of the object that contacts the print bed surface. This is because the characteristics on the bottom surface of the print bed resembled impressed characteristics found on the breech face area of firearms evidence. The aperture shear algorithm is utilized to compare striated markings found on the aperture shear section of the primer. Because the aperture shear algorithm is used for the comparison of striated markings, it was used on the top layer of the print bed that contacts the nozzle. This is because the characteristics on the top layer of the printed object that contact the nozzle were striated markings.

Once scans were uploaded to the TopMatch's incident analysis software, they were intercompared to each other using the TopMatch's pattern matching algorithms. The algorithm scored each comparison to a selected "reference" scan on a scale from 0.0 to 1.0 in terms of topographical similarity, where larger numbers indicate greater similarity. These comparison scores were then used for statistical analysis.

Print Bed Surface

The first area of the printer this study focused on is the print bed surface. The print bed surface is where the initial layer of the 3D printed object contacts the print bed. Because both the print bed surface and the PLA are heated, it is hypothesized that the thermoplastic properties of the PLA will allow it to inherit the characteristics of the print bed surface. The area of the printed object that contacts the print bed was scanned with the TopMatch-GS to produce a high-quality 3D image of the object's surface topography (Figure 5). Figure 5 highlights the granular

Figure 5. A TopMatch-GS scan of the bottom of the printed cartridge case that contacts the print bed. Multiple characteristics of the print bed that transferred to the bottom of the printed object can be easily observed.

characteristics that the 3D printed object inherits from the textured print surface on which it was printed. The lines present within Figure 5 are the 3D print path lines that the nozzle follows when creating the object layer by layer, these characteristics are present within all FDM 3D printed objects. Once the bottom surface of the object was scanned by the TopMatch system, the program had the user mask areas of the image that are suitable for algorithm comparison by highlighting the areas in a red color. This allowed the user to control what features the algorithm used to compare to other scans. When masking the scans of the print bed surface, the print path lines were not highlighted for algorithm analysis because they were present on the bottom layer of all FDM 3D prints. Figure 6 depicts how the bottom layer of the 3D printed objects were masked, with the areas that the algorithm will compare highlighted in a red color. The algorithm used for analysis of the print bed surface was Cadre's Breech Face 1.2 algorithm. Scores that the algorithm generates will be based solely on the characteristics within the red highlighting.

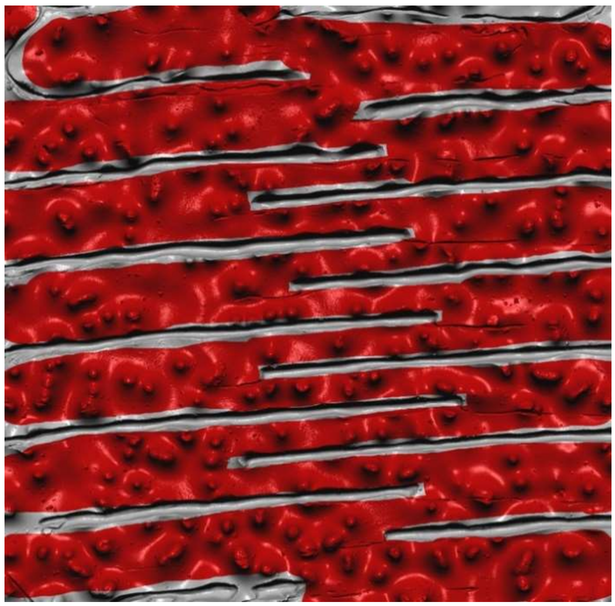

Figure 6. A focused TopMatch-GS scan of the bottom of the printed cartridge case that is appropriately masked for algorithm scoring analysis.

The print bed surfaces used in this study were Prusa Textured PEI Powder-Coated Spring Steel Sheet. The textured print bed surface was chosen due to its ease of printed object removal, as well as its durability. Although the textured print bed surfaces did not come with the Prusa MK4 printer, many other similar FDM printers come standard with textured print bed surfaces.

Hot End Nozzle

The second area of the printer this study focused on is the printer's hot end nozzle. The hot end nozzle is where heated filament is extruded from. The filament maintains constant contact with the nozzle as the object is being printed. During the manufacturing process, nozzles inherit characteristics incidental to their manufacturing process. Figure 7 highlights the microscopic

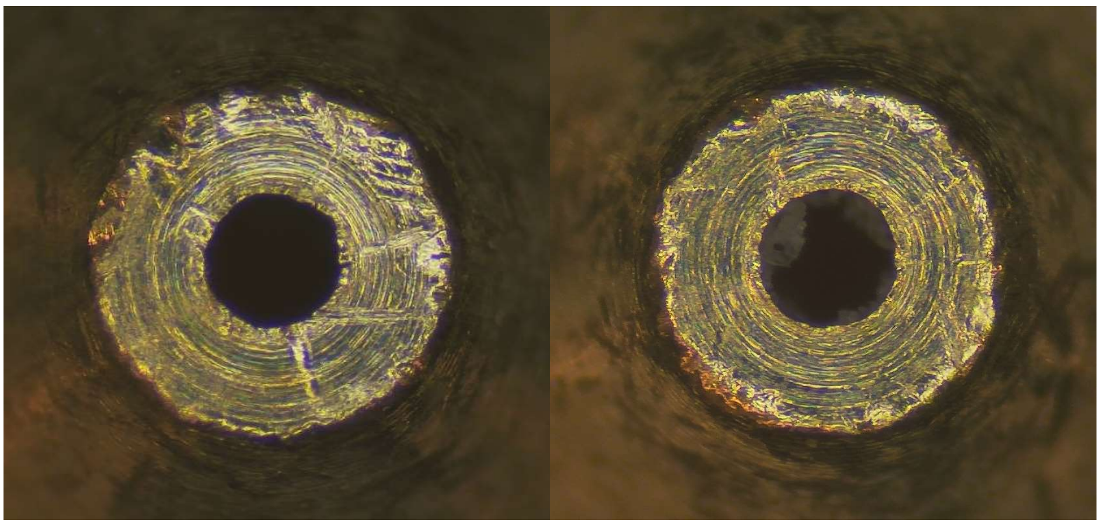

Figure 7. An image of the microscopic differences found between two unused hot end nozzles.

differences in the tips of unused hot end nozzles. It is hypothesized that the characteristics of the nozzle are transferred to the printed object as the nozzle moves to create the printed object. These markings are most commonly observed as striated marks on the top layer of the 3D printed object. The top layer of this study's printed object was designed to highlight these striated marks present in the 3D scanned image (Figure 8). Once the top of the object was scanned by the TopMatch system, the program had the user mask areas of the image that are suitable for algorithm comparison by highlighting the areas in a green color. Once again, this allowed the user to control what features the algorithm uses to compare to other scans. The algorithm used for analysis of the nozzle surface was Cadre's Aperture Shear 1.3 algorithm. Figure 8 depicts only a small, masked area of the printed object. This section of the object was chosen to be masked because it is a portion of the object that shows a non-overlapping area of nozzle striation. These sections of the print that depict non-overlapping areas of striated marks are theorized to be the best areas to use for comparison. This is because areas that do not overlap inherit the characteristics of the entire nozzle surface and are not destroyed by the normal print path. Since all these objects were printed from the same 3D modeled file, all prints would have a similar area of nozzle striation suitable for comparison purposes. All hot end nozzles used in this study were brass 0.4mm Prusa Nextruder nozzles. All hot end nozzles were new and bought directly from the Prusa website.

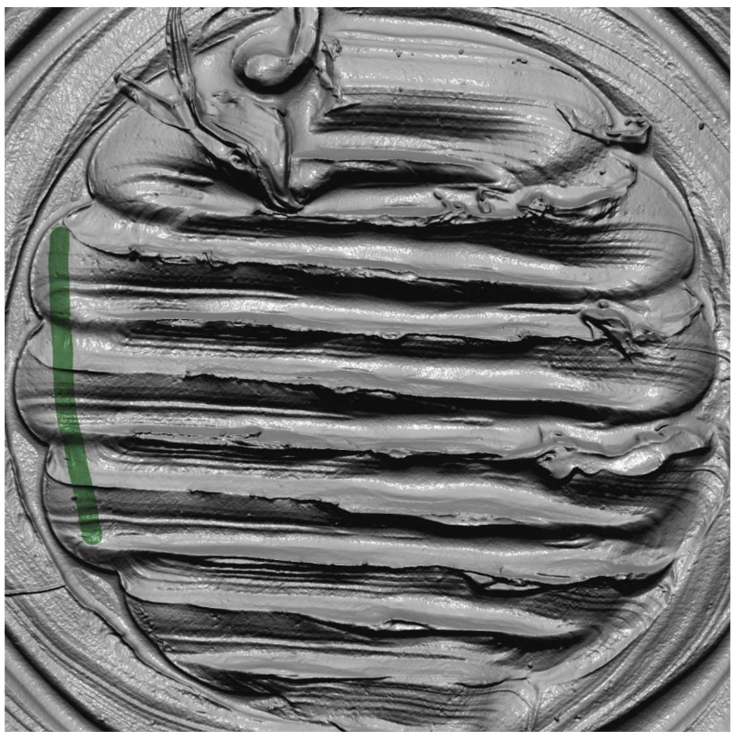

Figure 8. A TopMatch scan depicting the striations left by the nozzle of the 3D printer on the top layer of the object. The area in green is a selected "mask" of an area for the algorithm to use for comparison purposes.

Nozzle & Print Bed Wear

One of the most fundamental questions to consider when evaluating how viable a piece of evidence is for forensic toolmark examination is how its source changes over time with consistent use of the tool. In terms of 3D printed evidence, the tools and surfaces which the object inherits its characteristics from must be evaluated to see if their surfaces change significantly over time. To test this, three unused Prusa Nextruder nozzles were subjected to printing the same object using the same g-code 100 times in a row to determine if the nozzle surfaces changed significantly over time. These prints were also printed on three different print surfaces to determine if the print bed surface changed significantly over time as well. This resulted in 300 prints. 100 prints from each nozzle, with a different print surface corresponding to each nozzle. Every 10^{th} print, from the 1^{st} to the 100^{th} had the nozzle side and the print bed side scanned to visualize the surfaces. This resulted in 11 scans for each of the 3 nozzle surfaces and 11 scans for each of the 3 print surfaces.

Once the 3D scans of each of the print surfaces were complete, the scans were masked for algorithm analysis based on the surface type (nozzle or print bed). Once the scans were masked, the algorithm intercompared the scans for all of the nozzles and print beds coming from the same source. This provided a comparison score from 0.0 to 1.0 on how similar the surface topographies were. This was done to assess if there was a declining trend in comparison scores of prints coming from the same source over time, which would indicate the surface used to manufacture the object is wearing significantly.

Print Bed Surface and Nozzle Variability

This part of the study aimed to determine if the toolmarks present on the bottom and top surfaces of a 3D printed object are distinct enough to be used in forensic analysis. In this part of the study, 10 different hot end nozzles and 10 different print bed surfaces were used. 15 prints were conducted per nozzle and per print bed surface. The first 10 prints for each surface were printed consecutively with no adjustment, but for the last 5 prints, the nozzle and print bed surfaces were removed and then reapplied to the 3D printer. This was done to simulate normal working conditions when printing objects. All prints for this part of the study used the same gcode to print the object.

Since the nature of the design was double sided, each top and bottom surface of the 3D printed object was scanned. This created 150 3D scans for the bottom surface that contacted the print bed and 150 scans for the top surface that contacted the hot end nozzle. This resulted in a total of 300 3D scans with a known origin. Each scan was manually masked and intercompared to all other scans of the same surface (nozzle or print bed) using the TopMatch's 3D comparison algorithms. As mentioned previously, the breech face algorithm was utilized for the scans that contacted the print bed surface, and the aperture shear algorithm was used for the scans that contacted the hot end nozzle. Once all scans were uploaded and the algorithm had inter-compared all scans, the data was exported to conduct data analysis.

Open-Set Unknown Comparisons

In addition to the 150 prints of known origin, 25 more objects were printed by another individual, with the origins of the objects being known only to that individual. These 25 prints had each side scanned, for a total of 50 scanned surfaces, 25 of the print bed surface and 25 of the nozzle surface. These scans were compared to scans of known origin in an open set design, meaning not all of the objects of unknown origin were guaranteed to be identified to a known. These scans were uploaded to the TopMatch's incident analysis program for visual comparison and algorithm analysis. Once all scans were uploaded and the algorithm had cross-compared all scans, the algorithm's scores were used as a triage tool to quickly identify potential same source objects. The scans with the highest comparison scores were visually compared, and conclusions were made for each of the 50 scans. Comparisons between the known objects and the unknown objects had their conclusions plotted into a confusion matrix. A confusion matrix is a performance measurement table that visualizes the number of true positives, true negatives, false positives, and false negatives (Kulkarni et al., 2020). Figure 9 depicts a confusion matrix.

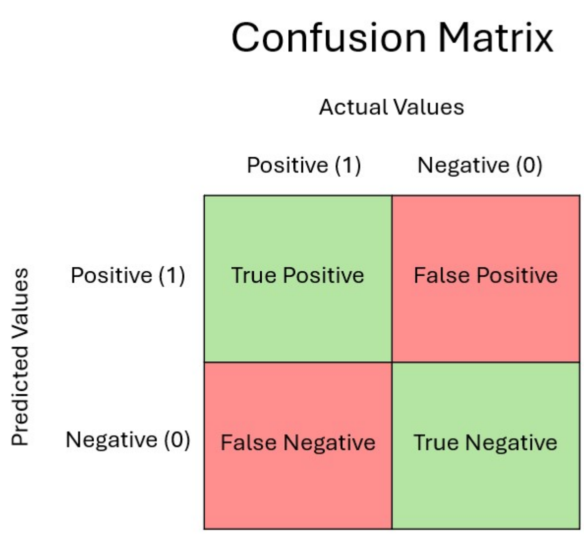

Figure 9. An example of a confusion matrix.

Results & Discussion

Print Bed & Nozzle Wear

For each of the three nozzles and print beds used to evaluate the level of wear present, scores were plotted to determine if they trended downward over time. A downward trend of algorithm scores would indicate that the surface is wearing significantly over time. To visualize this, the first print for each surface was compared to every 10^{th} print, up to the 100^{th} print. Figure 10 depicts the breech face algorithm scores of print bed B, side A, section L. As seen in Figure

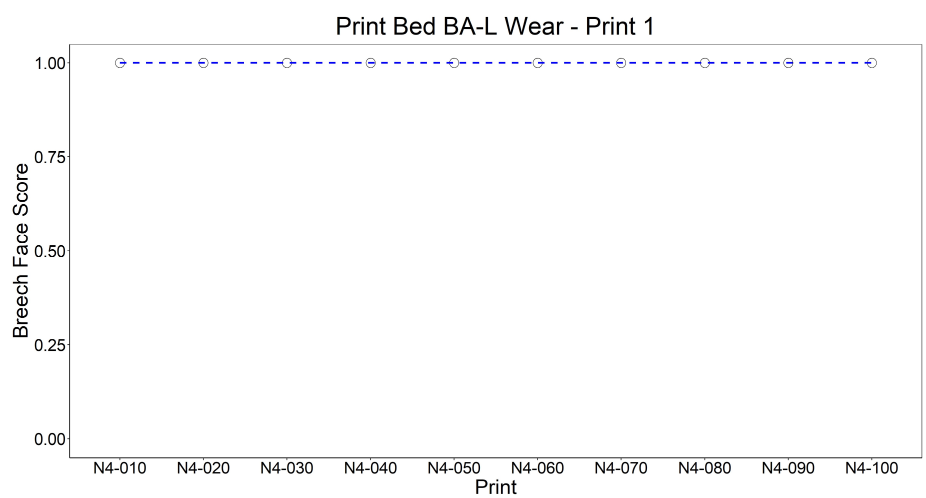

Figure 10. A graph comparing the first print of print bed B, side A, section L to every 10th print, up to the 100th print.

10, the first print compared to all prints retained a score of around 0.9999. This indicates that the print bed surfaces do not wear significantly over time. This trend was seen throughout all three of the tested print bed surfaces. Figure 11 depicts the breech face algorithm scores of print bed B, side A, section M. Figure 12 depicts the breech face algorithm scores of print bed B, side A, section N. Since all of the three different print bed surfaces retained high algorithm scores over time, it can be inferred that the print surface of the printer does not change significantly over time to impact the toolmarks found on the bottom layer of 3D printed objects.

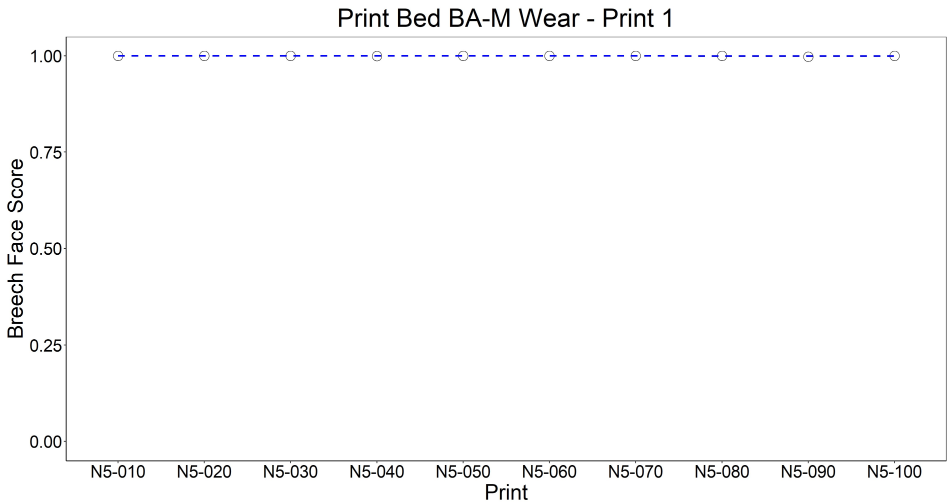

Figure 11. A graph comparing the first print of print bed B, side A, section M to every 10th print, up to the 100th print.

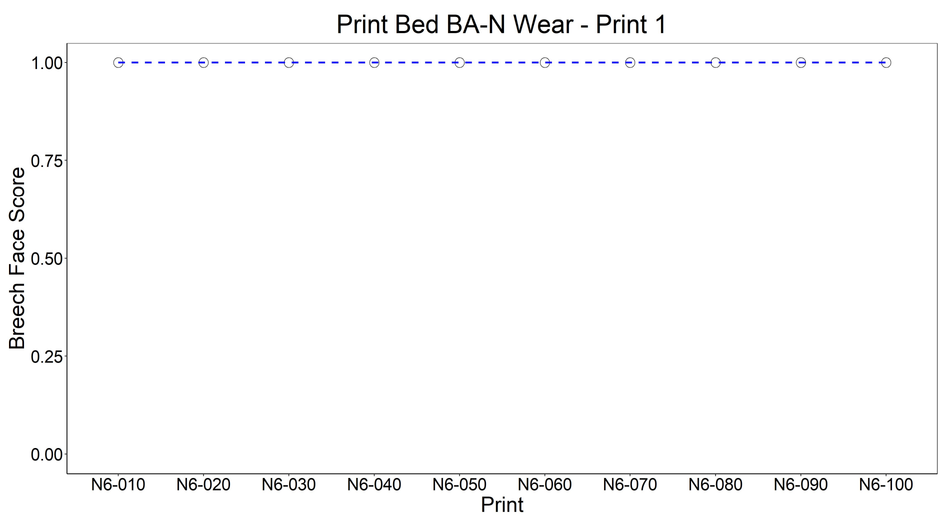

Figure 12. A graph comparing the first print of print bed B, side A, section N to every 10th print, up to the 100th print.

The nozzle surfaces were evaluated using the same methodologies as the print bed surfaces, however the algorithm used for the nozzle surfaces did not provide the same level of consistent scoring as the algorithm used for the print bed surfaces. It is hypothesized that since the algorithm is traditionally used for very fine and deep striated marks, the shallower striated toolmarks found on the nozzle surface of the prints were not as ideal for Cadre's aperture shear algorithm comparison. Algorithm scores were still used for objective comparison of all nozzle surfaces in this study, but visual comparisons were also used to support the conclusions of this study. Figure 13 depicts a graph of the aperture shear algorithm scores for nozzle 4. Although the nozzle algorithm scores are generally much lower than the print bed algorithm scores, there is still the ability to observe a trend indicating if the surfaces wear significantly over time. The

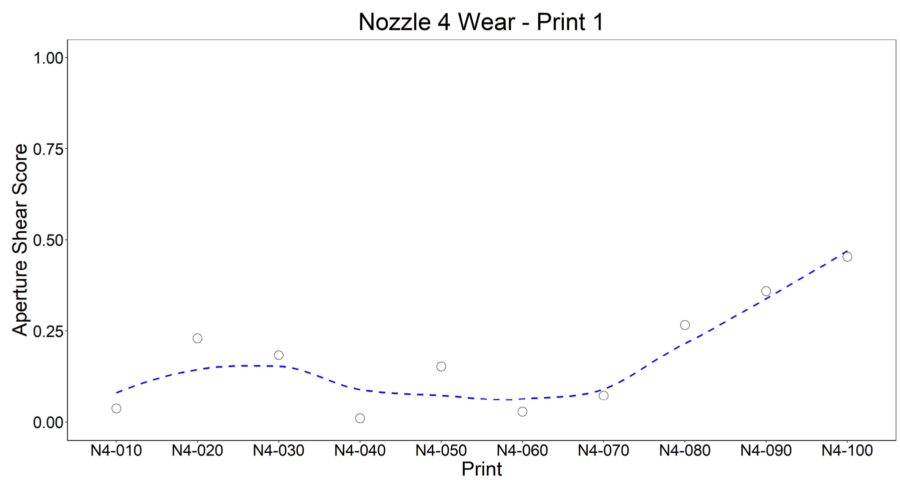

Figure 13. A graph comparing the first print of nozzle 4 to every 10th print, up to the 100th print.

scores for nozzle 4 seen in Figure 13 do not suggest that there is an indication of the surface wearing over time. Figure 14 also depicts images of visual comparisons from the first print of nozzle 4 compared to the 100th print of nozzle 4. Figure 13 focuses on three different areas of comparison where sufficient agreement can be seen between the two comparisons, the

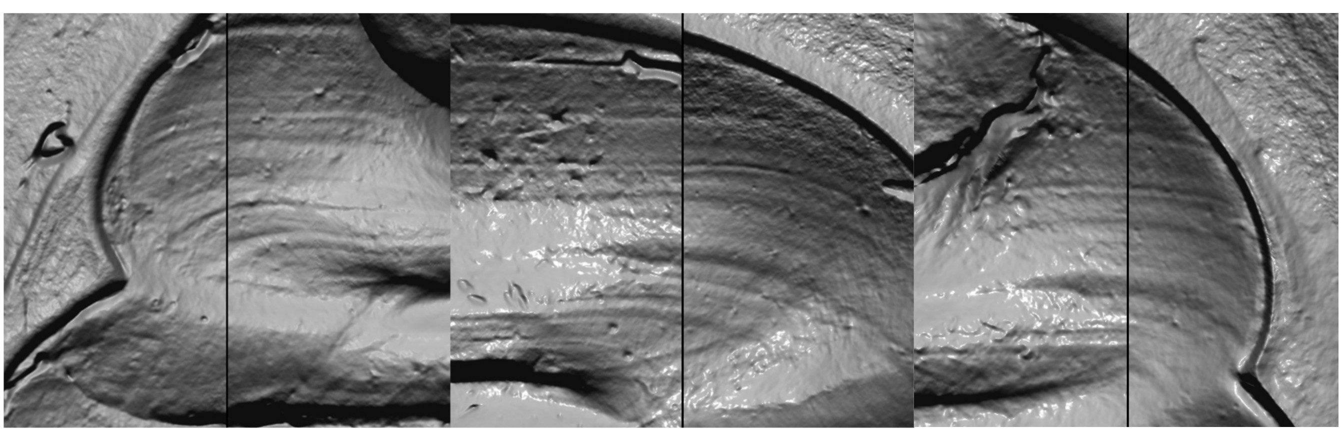

Figure 14. Images of a visual comparison between the 1st and 100th prints made by nozzle 4. Three different areas containing sufficient characteristics were viewed, the left (left), top (middle), and right (right) sides of the surface.

left, top, and bottom sides of the nozzle surface. Similar trends were seen between the three nozzles used for the wear portion of the study. Figure 15 depicts the aperture shear algorithm scores for nozzle 5. Although scores may seem to be trending downward, there is no significant

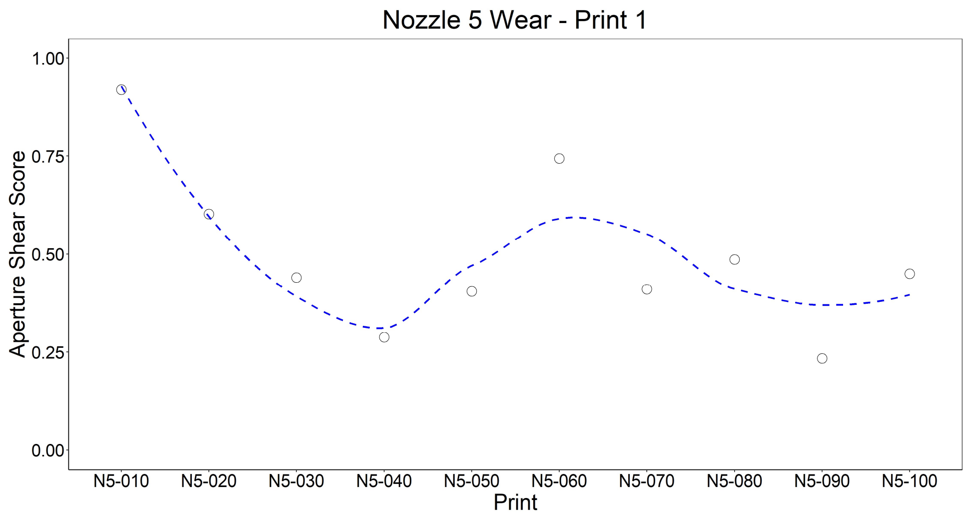

Figure 15. A graph comparing the first print of nozzle 5 to every 10th print, up to the 100th print.

trend to indicate that the surface is wearing over time. Similar to nozzle 4, visual comparisons were done with nozzle 5, and sufficient agreement was easily found between the 1st and 100th prints. This continues to indicate that these surfaces do not wear over time. Figure 16 depicts

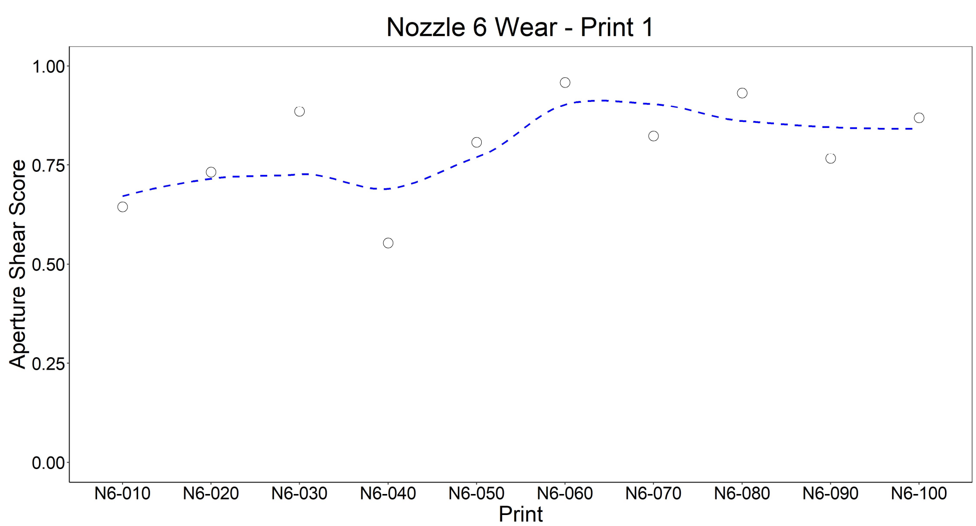

Figure 16. A graph comparing the first print of nozzle 6 to every 10th print, up to the 100th print.

a graph of the aperture shear algorithm scores for nozzle 6. Again, visual examination of the algorithm score graphs suggests these surfaces do not wear significantly over time, and visual comparisons were conducted to corroborate this conclusion.

In conclusion, there is no indication that the nozzle surfaces and the print bed surfaces wear significantly over time. Using algorithm scoring and visual comparisons of the print surfaces corroborates this conclusion.

Print Bed Surface and Nozzle Variability

The similarity scores that the algorithm provides are a quantifiable measure of the similarity of two surface topographies. This feature is essential for a quantitative analysis of similarity, as opposed to traditional subjective analysis. The print bed surface of the printed objects had 14 same-source and 135 different-source comparisons each (recall, 15 objects were printed across ten different print beds). The print nozzle surfaces of the printed objects also had 14 same-source and 135 different-source comparisons each. When intercompared to each other, this resulted in a total of 11,175 comparison scores for print bed surfaces and 11,175 comparison scores for nozzle surfaces. Using data from these comparisons, receiver operating characteristics (ROC) curves were used to evaluate the ability of the TopMatch's algorithms to differentiate between same source and different source 3D printed surfaces (Fawcett, 2006). ROC curves were generated for both print surface comparison data as well as nozzle comparison data. The area under the curve (AUC) metric was used to identify the probability of a randomly selected same source comparison having a higher algorithm score than a randomly selected different source comparison. Figure 17 depicts the ROC curve and the AUC score for all 11,175 print bed comparisons. The print bed comparisons received an AUC score of 1.00, meaning that the algorithm was correctly able to distinguish between same source and different source comparisons 100% of the time, using only algorithm scores and no visual comparisons. These data objectively suggest that toolmarks present on the print bed surface of a printed object can be used to identify and exclude objects coming from a certain source.

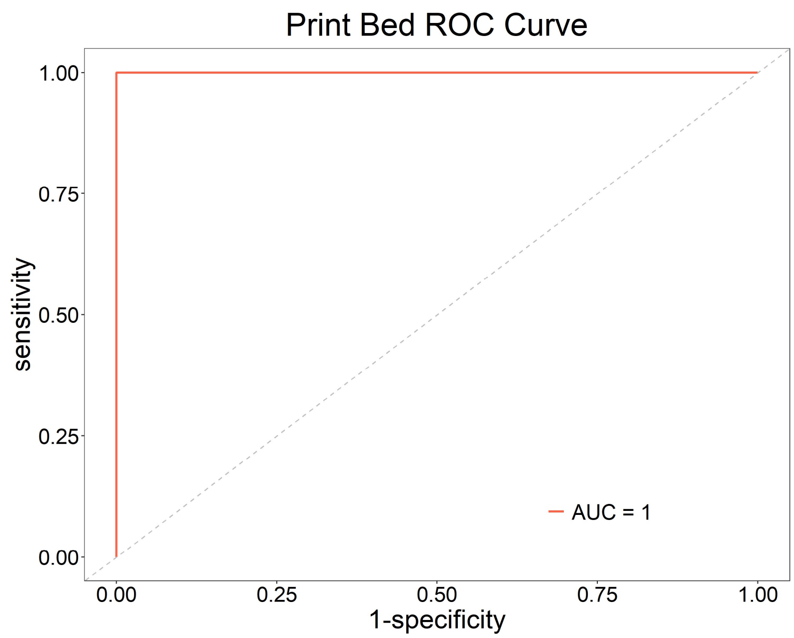

Figure 17. A ROC curve and AUC score generated for all 11,175 print bed comparisons.

A ROC curve and AUC score were also generated for the nozzle comparisons. Figure 18 depicts the ROC curve and AUC score for all of the 11,175 nozzle comparisons. The AUC score for all of the nozzle comparisons was 0.86, meaning that the algorithm was correctly able to distinguish between same source and different source comparisons 86% of the time. It is important to note that this statistic is calculated using only the algorithm's scores of the surface topographies and no visual examination was used.

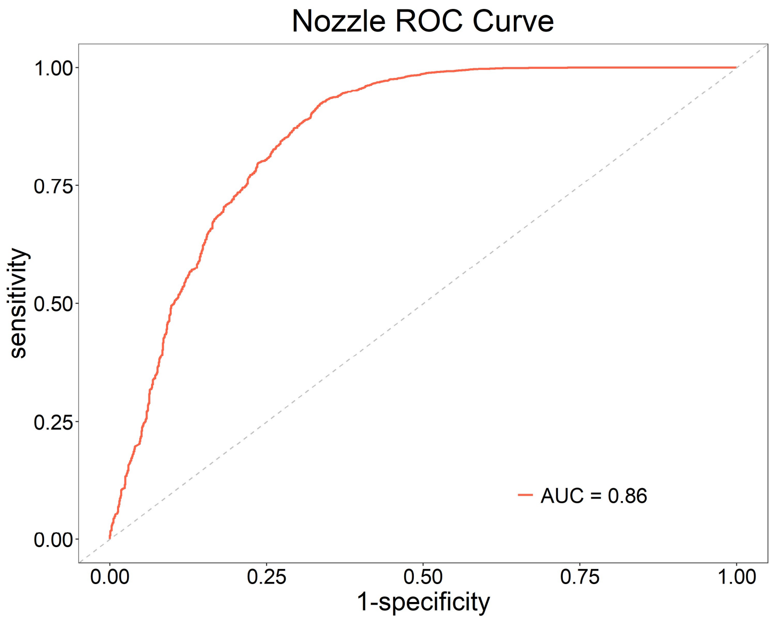

Figure 18. A ROC curve and AUC score generated for all 11,175 nozzle surface comparisons.

To further understand if certain print beds and nozzles performed differently from others, ROC curves and AUC scores were calculated for each individual nozzle and print bed tested in this study. Figure 19 depicts all 10 ROC curves and AUC scores calculated for the print bed surface combined onto one plot. Since the AUC score of all print surfaces combined was 1.00, each individual print bed surface also has an AUC score of 1.00. This suggests that all print bed surfaces consistently left enough characteristics for the algorithm to discern between same source and different source comparisons. Figure 20 depicts the ROC curves and AUC scores calculated for all 10 of the nozzle surfaces combined onto one plot. As seen in Figure 20, the AUC scores from different nozzles ranged from a high of 0.95 to a low of 0.74, with only two nozzles (N10 & N12) falling below an AUC of 0.84. Although a wide range of AUC scores is present within the nozzle comparisons, these data suggest that nozzles that may not mark as well still leave characteristics that are distinct enough that the algorithm was able to correctly discern between same source and different source comparisons at least 74% of the time. Similar to traditional

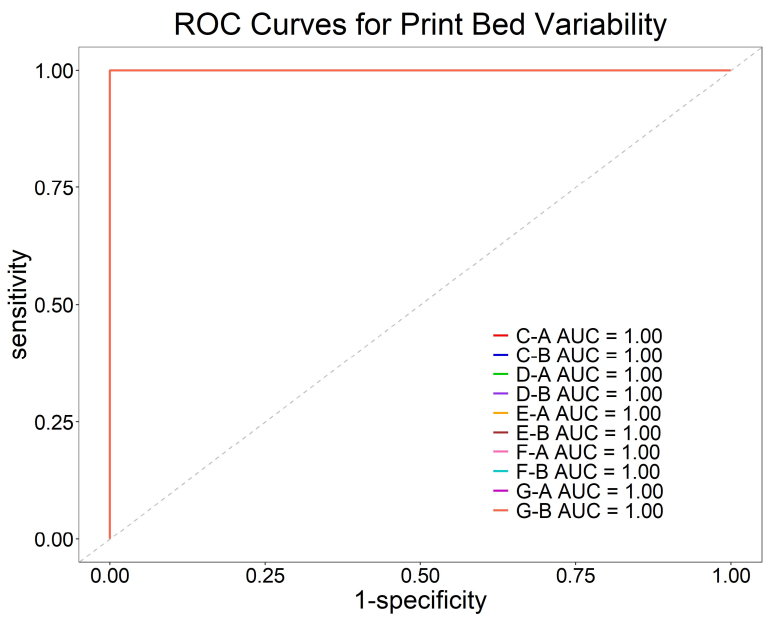

Figure 19. A combined plot depicting all ROC curves and AUC scores for each individual print bed surface.

toolmark examination, these data provide insight into how different surfaces the object contacts during printing may have areas that leave characteristics more consistently than others.

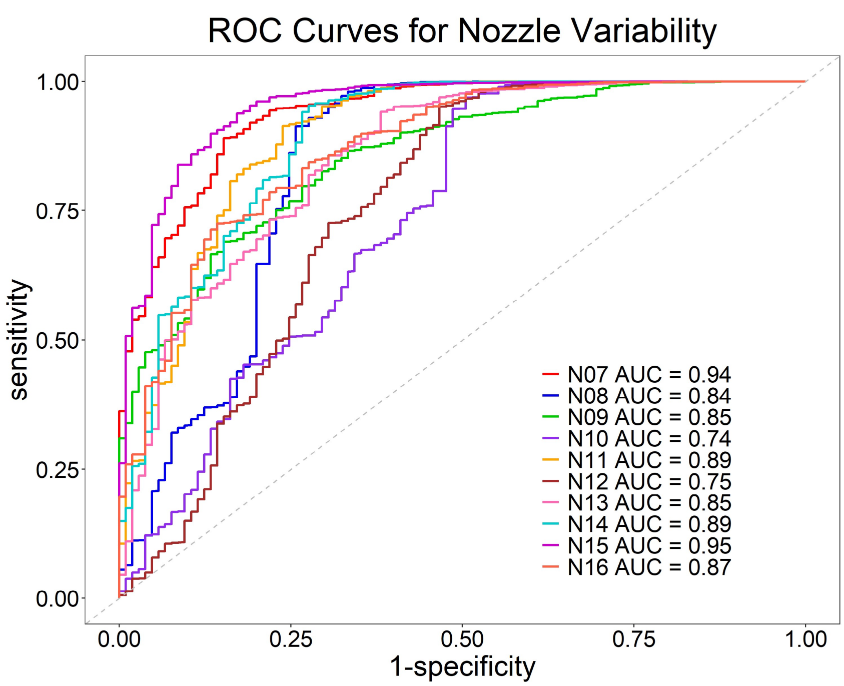

Figure 20. A combined plot depicting all ROC curves and AUC scores for each individual nozzle surface.

To further understand the variability of the AUC scores for the print bed surfaces and nozzle surfaces, algorithm scores between the objects of a known same source were plotted using box plots. This analysis allows for the visualization of variabilities present within 3D printed objects of the same source. Figure 21 depicts the box plot of the same source comparison scores

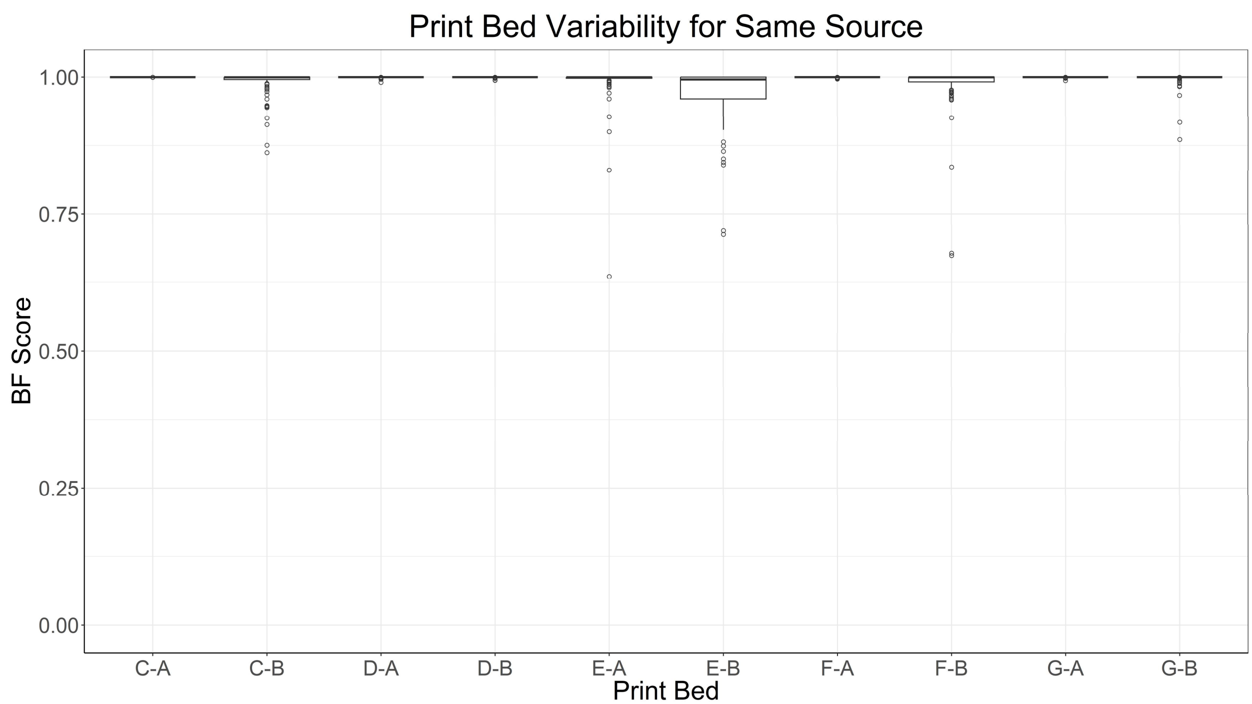

Figure 21. A box plot depicting the variability of algorithm scores of same source comparisons within each individual print bed surface.

for the print bed surfaces. As shown in Figure 21, there is not much variability in the same source comparison algorithm scores for the print bed surfaces, with the exception of a few outliers. Although print bed E-B had the most variability in same source comparison scores, the variability did not affect the algorithm's ability to distinguish between same source and different source comparisons. These data depict that the variability between same source print bed comparisons is not significant enough to have an effect on the ability to make sound conclusions on toolmarks found on the bottom layer of 3D printed objects.

Figure 22 depicts the box plot of the same source comparison scores for the nozzle surfaces. As seen in Figure 22, the variability in algorithm scores for same source nozzle comparisons is much greater than that of the print bed comparisons. This was expected, as the nozzle comparisons in this study did not score as well as the print bed comparisons. This box plot also depicts two nozzles that had the highest variability in same source comparison scores,

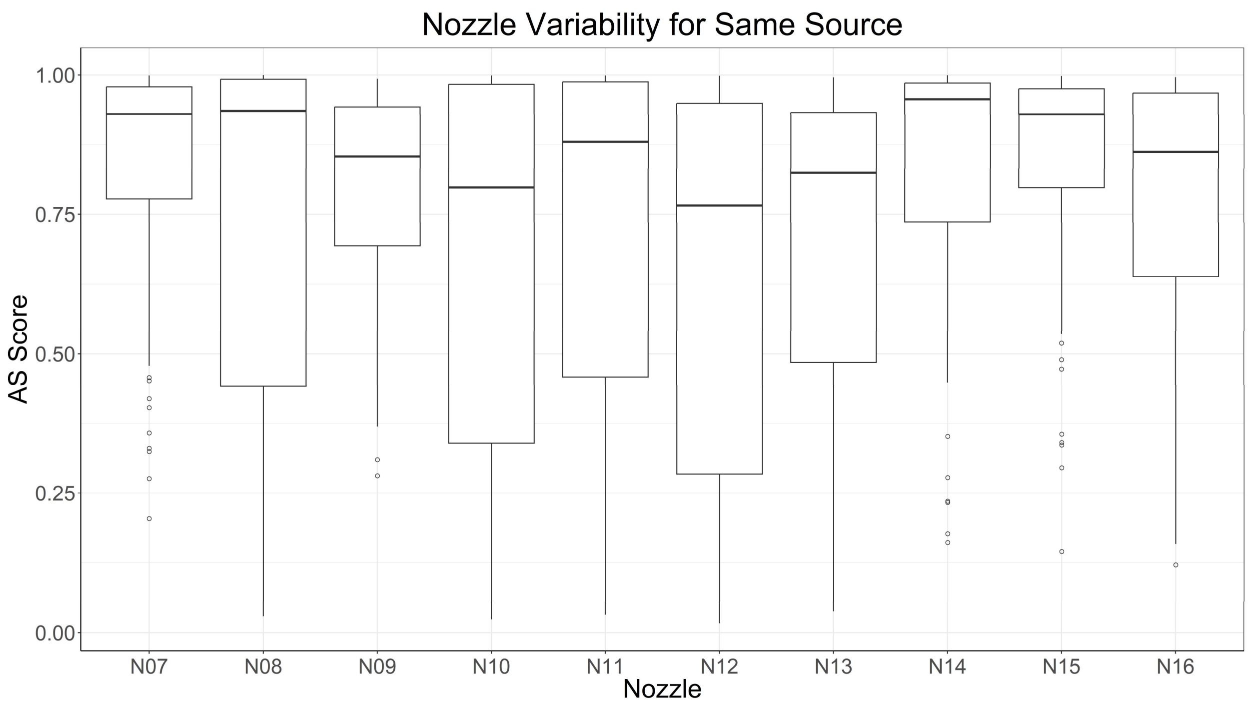

Figure 22. A box plot depicting the variability of algorithm scores of same source comparisons within each individual nozzle surface.

nozzle N10 and nozzle N12. Recall that both nozzle N10 and nozzle N12 also had the lowest AUC scores for their individual ROC curves, indicating that the markings on these nozzles may be harder to identify than others. Contrary to the previous two nozzles, nozzle N07 and nozzle N15 had the lowest same source score variability with the two highest AUC scores. This may indicate that these nozzles may leave more distinct and identifiable markings on 3D printed evidence.

Overall, the data collected indicates that toolmarks present on textured print bed surfaces and nozzle surfaces are distinct enough to be used for source conclusions. The data collected also indicates that there is minimal variability in markings present on the bottom layer of a printed object that contacted the Prusa textured print bed, where there is more variability in striated markings present on the top layer of a printed object that contacts the nozzle. Although the variability in nozzle surface comparison scores impacted the algorithm's ability to distinguish between same and different sources, the data from this study still suggests that nozzle surface comparison is viable for toolmark comparison analysis.

Open-Set Unknown Comparisons

After assessing print bed and nozzle variability, an unknown set of 25 print bed objects and 25 nozzle objects were printed and evaluated for conclusion accuracy in a scenario that would resemble traditional casework. Comparisons between the known objects and the unknown objects had their conclusions plotted into a confusion matrix. The confusion matrix allows for the visualization of the number of true positive, true negative, false negative, and false positive examiner conclusions. Figure 23 depicts the overall confusion matrix scores from all 50

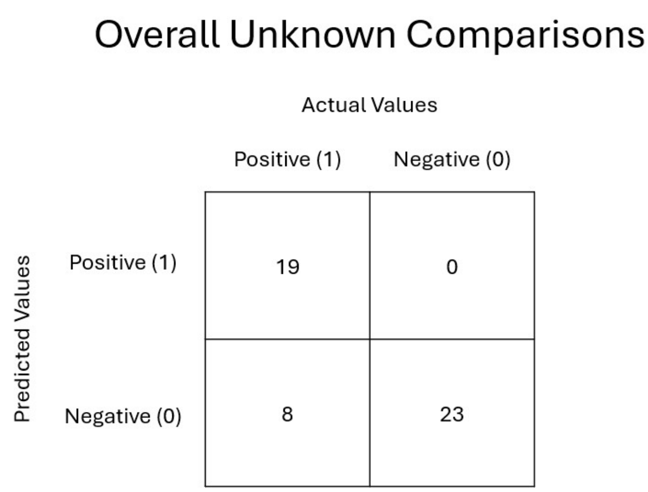

Figure 23. A confusion matrix plotting all conclusions made in the open-set study.

unknown comparisons. As seen in Figure 23, there were a total of 19 true positive conclusions, 23 true negative conclusions, 8 false negative conclusions, and 0 false positive conclusions. This totals an overall correct conclusion rate of 84%. To gain a deeper understanding of the conclusions made, confusion matrices were created for both print bed surfaces and nozzle surfaces individually.

Figure 24 depicts the confusion matrix scores for only the print bed surface conclusions. As seen in Figure 24, there were a total of 10 true positive conclusions, 15 true negative conclusions, 0 false negative conclusions, and 0 false positive conclusions. This totals an overall correct conclusion rate of 100%. This was expected, as the print bed surfaces mark more

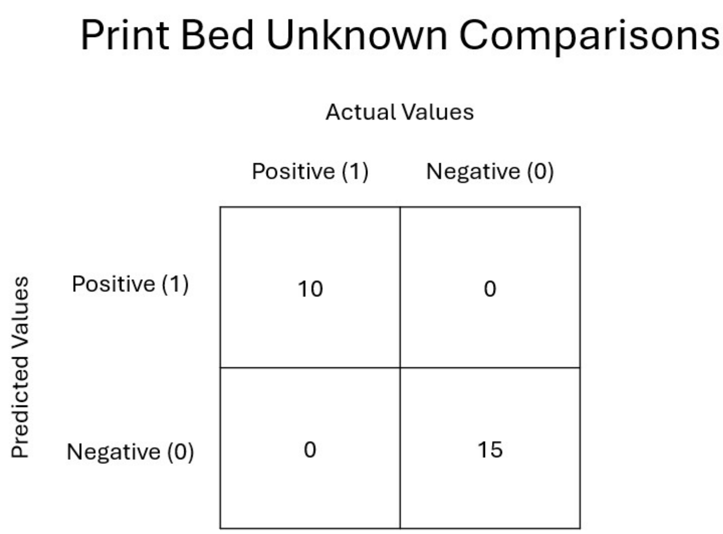

Figure 24. A confusion matrix plotting the conclusions made for the print bed comparisons.

consistently and with less variability than that of the nozzle surfaces. Figure 25 depicts the confusion matrix scores for only the nozzle surface conclusions. As seen in Figure 25, there were a total of 9 true positive conclusions, 8 true negative conclusions, 8 false negative conclusions, and 0 false positive conclusions. This totals an overall correct conclusion rate of 68%. The visual comparisons of the nozzle surfaces were much more difficult than the print bed surface

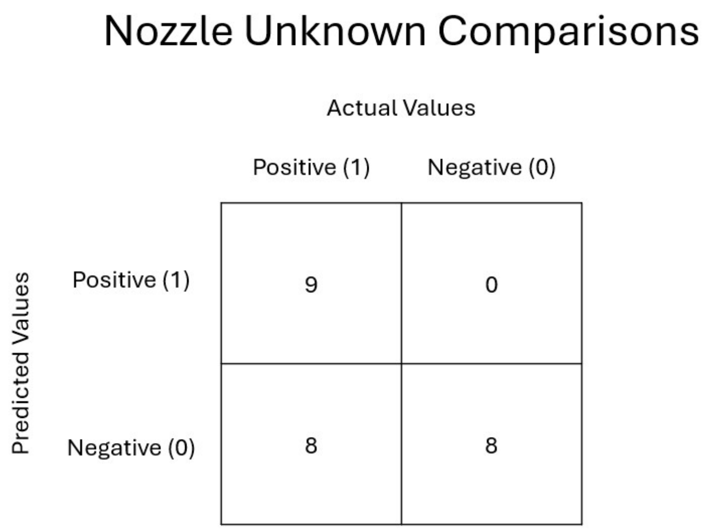

Figure 25. A confusion matrix plotting the conclusions made for the nozzle surface comparisons.

comparisons which was expected based on the ROC curve analysis. It is also important to note that unknown prints coming from the same unknown source were able to be correctly correlated 100% of the time, even if their comparison to the known source was incorrect. Figure 26 depicts a visual comparison with an unknown nozzle surface (left) compared to a known nozzle surface

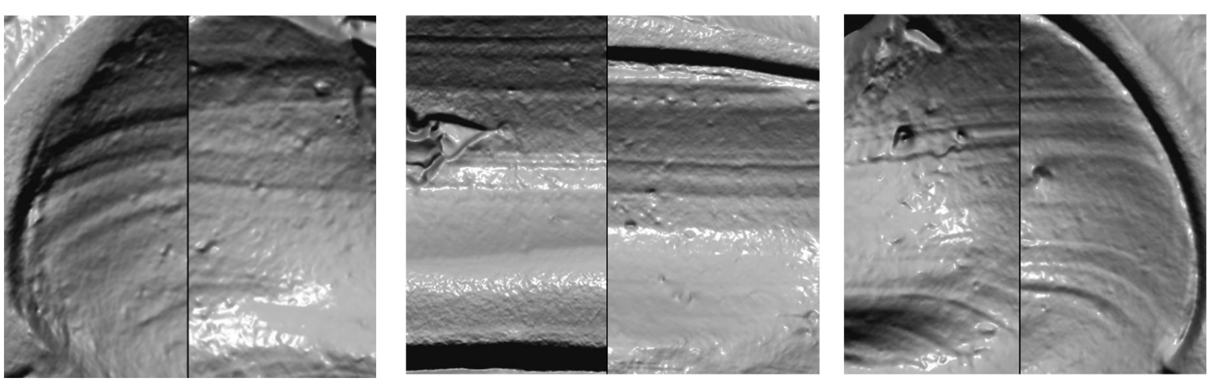

Figure 26. Images of a visual comparison between an unknown nozzle surface (left side) and known nozzle surface of N10 (right side). Three different areas containing significantly different characteristics were viewed, the left (left), top (middle), and right (right) sides of the surface.

(right) of nozzle N10. The unknown nozzle surface in Figure 26 was eliminated from being made by nozzle N10, but the ground truth of the comparison indicated that they came from the same source. Markings on the eight falsely eliminated unknown nozzle surfaces were significantly different from the surface of known origin. There may be several reasons for this significant difference in characteristics between the known and unknown prints.

The first explanation of these significantly different characteristics was that some of the printed objects were printed with different gcode. This different gcode allowed for printing multiple objects at the same time to improve the efficiency of the printing process. This change of the printed file may have slightly changed the print path of the nozzle, leaving different characteristics on the printed object. To investigate this, two different objects were printed using both different gcode files to determine if the change in gcode had an effect on the striated characteristics present on the nozzle surfaces. Figure 27 depicts two different printed objects printed with the same nozzle, but with slightly different gcode. As seen in Figure 27, the striated markings present on the nozzle surface of the two objects printed with different gcode had

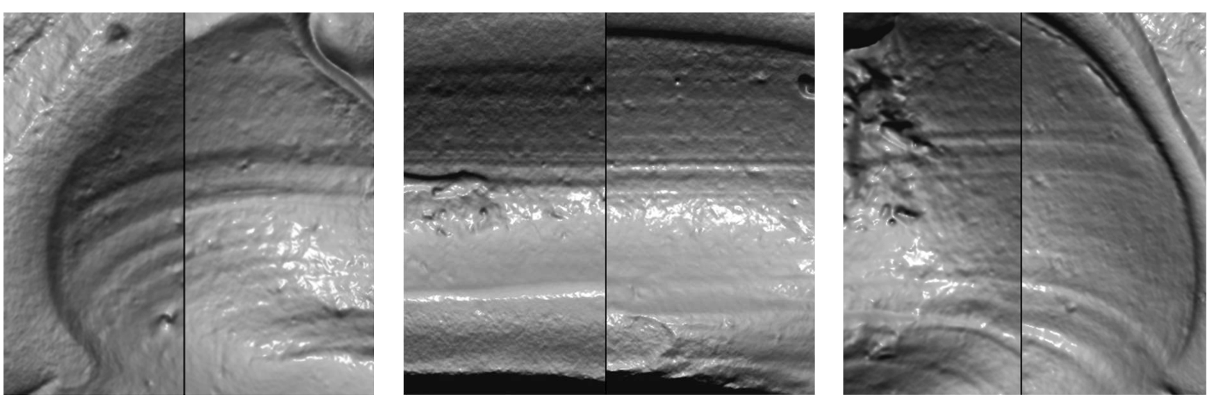

Figure 27. Images of a visual comparison between two nozzle surfaces printed with slightly different gcode. Three different areas containing similar characteristics were viewed, the left (left), top (middle), and right (right) sides of the surface.

enough sufficient agreement to make an identification. This indicates that the minor change in gcode did not have a significant effect on the toolmarks present on the nozzle surfaces of the objects. The change in gcode also did not affect the print bed surface of the objects because characteristics inherited by the print bed surface are influenced by where the object is printed on the print bed surface as opposed to the nozzle path.

The second explanation relates to the mechanical nature of the printer itself. There was a significant amount of time between the printing of the known prints and the unknown prints. During this period, several other prints unrelated to this study were conducted. It is possible that wear and degradation of the mechanical parts of the 3D printer occurred between the time of printing the known and unknown prints. However, this does not explain how some unknown nozzle surfaces were able to be easily identified and some were not able to be identified. The cause of the significant differences in markings on some of the unknown print surfaces is currently unknown and requires further research.

Overall, the conclusions made in this open-set blind comparison study suggest that examination of toolmarks present on 3D printed objects is still viable for forensic analysis. However, different files used to print the objects may have an effect on toolmarks present on the nozzle surface of the printed objects, and normal wear of the mechanical parts of the 3D printer may also influence markings found on the 3D printed object. Further expansion of this study should include a design where the same file is used to print all 3D printed objects for comparison. Further research is also needed on how much printer mechanical part degradation affects markings found on 3D printed objects.

Limitations

The data from this study suggests that toolmarks imparted onto 3D printed objects during the 3D printing process can be used to draw source conclusions. However, only one 3D printer, a Prusa MK4, was used to print all 3D printed objects. Even though different print bed surfaces and nozzles were used to represent several printers, many other 3D printer manufacturers may use different techniques to manufacture their print surfaces or hot end nozzles. Differences in manufacturing methods of 3D printer parts may lead to different, or even no characteristics at all. Another limitation is that only one type of filament was used. Although PLA is one of the most common 3D printer filaments, different plastics may have different properties. This could change the number of characteristics that are transferred from the printer to the object, thus changing the effectiveness of identifying the source of the print.

Further limitations of this research relate to the algorithms used during this study. Cadre's Breech Face 1.2 algorithm is intended to be used in the analysis of microscopic, impressed characteristics on the primer surface of fired cartridge cases. Cadre's Aperture Shear 1.3 algorithm is intended to be used in the analysis of microscopic, striated markings on the primer surface of fired cartridge cases. Although the algorithm scoring performed fairly well in differentiating between same and different source conclusions for both print bed and nozzle surfaces, it is important to note that these algorithms were not designed for the analysis of 3D printed evidence.

Other limitations of this study are based on the design of the study. First, the sample size included only 15 prints per nozzle and print bed surface. The average 3D printer nozzle can typically handle hundreds of prints before it needs to be replaced. Secondly, only 100 small prints were conducted for the wear portion of the study. Printers often handle much larger, and more frequent printed objects. The results of the surface wear portion of the study may not be as generalizable to printer surfaces that have withstood creating much larger, and much more frequent 3D printing objects.

Another limitation of this study is that only textured print surfaces were used. Although textured print surfaces are popular, smooth print surfaces are also used to manufacture 3D printed objects. Figure 28 shows a 3D scan of the bottom layer of an object printed on a smooth print surface. No significant markings were observed on the objects printed on the smooth print surfaces. The diagonal lines seen in Figure 28 have even spacing and may be observable on all smooth print bed surfaces manufactured by Prusa. However, previous research suggests that markings found on smooth print surfaces after their manufacture are inherited by the printed object (Aronson et al., 2019). Overall, more research must be conducted before determining if characteristics found on the bottom layer of 3D printed objects printed on smooth print surfaces are distinct enough to be used for source conclusions.

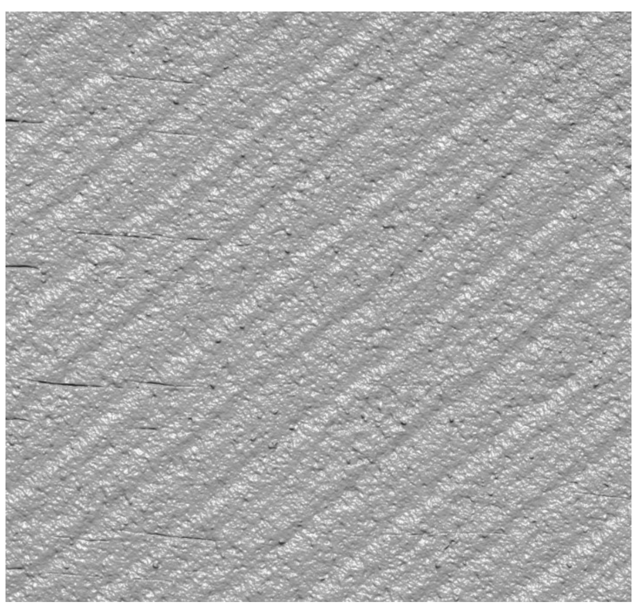

Figure 28. A TopMatch-GS scan of the bottom of an object that was printed on a smooth print surface.

Conclusion

Data from this study not only suggests that the tools and surfaces that a 3D printed object inherits its characteristics from do not degrade significantly over time, but also suggests toolmarks present on 3D printed objects can be used to identify or exclude if an object came from a certain source. Impressed characteristics found on the bottom layer of the printed object that contacts the print bed surface and striated markings found on the top layer of the printed object that contacts the nozzle surface produced the best characteristics for comparison purposes. Utilizing surface topography similarity algorithms allowed for statistical and objective analysis of 3D printed surface topographies to aid in determining that they were suitable for forensic analysis.

The results of this study are significant for the field of toolmark examination because 3D printing technology is increasingly being used to manufacture firearms and illegal firearm components. Although further research in the field of 3D printed object toolmark analysis is needed, the data from this study strongly suggests the possibility of source identification using toolmarks present on 3D printed objects.

Recall that other 3D printer manufacturers may use different techniques to manufacture their print surfaces or hot end nozzles, which may leave different or no characteristics at all. Continued work in the field of 3D printed object toolmark analysis could analyze objects printed using different models of 3D printers to determine if those objects can also be used for forensic analysis. Future work may also include black box studies of 3D printed object toolmark analysis, designed to evaluate examiner conclusions. This would aid in the implementation of these methods into the field of firearm and toolmark analysis.

References

Vizzard, W. J. (1999). The gun control act of 1968 symposium: gun control. *Saint Louis University Public Law Review*, *18*(1), 79–98.

Pavlovich, S., & Garrison, K. (2023). An exploratory study of topographical signatures within 3D fused deposition modelling using Polylactic Acid (PLA) filament. *Forensic Science International*, *349*, 111740. https://doi.org/10.1016/j.forsciint.2023.111740

Aronson, A., Elyashiv, A., Cohen, Y., & Wiesner, S. (2021). A novel method for linking between a 3D printer and printed objects using toolmark comparison techniques. *Journal of Forensic Sciences*, *66*(6), 2405–2412. https://doi.org/10.1111/1556-4029.14825

Su, A., & Al'Aref, S. J. (2018). History of 3D Printing. In *3D Printing Applications in Cardiovascular Medicine* (pp. 1–10). Elsevier. https://doi.org/10.1016/B978-0-12-803917-5.00001-8

Ngo, T. D., Kashani, A., Imbalzano, G., Nguyen, K. T. Q., & Hui, D. (2018). Additive manufacturing (3D printing): A review of materials, methods, applications and challenges. *Composites Part B: Engineering*, *143*, 172–196. https://doi.org/10.1016/j.compositesb.2018.02.012

Przekop, R. E., Gabriel, E., Pakuła, D., & Sztorch, B. (2023). Liquid for Fused Deposition Modeling Technique (L-FDM)—A Revolution in Application Chemicals to 3D Printing Technology: Color and Elements. *Applied Sciences*, *13*(13), 7393. https://doi.org/10.3390/app13137393

Heard, B. J. (2008). *Handbook of Firearms and Ballistics: Examining and Interpreting Forensic Evidence* (1st ed.). Wiley. https://doi.org/10.1002/9780470694589

Greenberg, A. (2014, October 1). *The $1,200 machine that lets anyone make a metal gun at home*. Wired. https://www.wired.com/2014/10/cody-wilson-ghost-gunner/

AFTE. (n.d.). AFTE theory of identification as it relates to toolmarks. hthttps://afte.org/about-us/what-is-afte/afte-theory-of-identification

Mattijssen, E. J. A. T. (2020). Interpol review of forensic firearm examination 2016-2019. *Forensic Science International: Synergy*, *2*, 389–403. https://doi.org/10.1016/j.fsisyn.2020.01.008

Baldwin, D. P., Bajic, S. J., Morris, M. D., & Zamzow, D. S. (2023). A study of examiner accuracy in cartridge case comparisons. Part 1: Examiner error rates. *Forensic Science International*, *349*, 111733. https://doi.org/10.1016/j.forsciint.2023.111733

Baldwin, D. P., Bajic, S. J., Morris, M. D., & Zamzow, D. S. (2023). A study of examiner accuracy in cartridge case comparisons. Part 2: Examiner use of the AFTE range of conclusions. *Forensic Science International*, *349*, 111739. https://doi.org/10.1016/j.forsciint.2023.111739

Leon, K. N. (2019). Beyond the Single-Use Plastic Gun: The Need to Make 3d-Printed Gun Laws Shatterproof. *Houston Law Review*, *57*(2), 437–466.

Trincat, T., Saner, M., Schaufelbühl, S., Gorka, M., Rhumorbarbe, D., Gallusser, A., Delémont, O., & Werner, D. (2022). Influence of the printing process on the traces produced by the discharge of 3D-printed Liberators. *Forensic Science International*, *331*, 111144. https://doi.org/10.1016/j.forsciint.2021.111144

Honsberger, H., Rhumorbarbe, D., Werner, D., Riva, F., Glardon, M., Gallusser, A., & Delémont, O. (2018). How to recognize the traces left on a crime scene by a 3D-printed Liberator?: Part 1.

Discharge, exterior ballistic and wounding potential. *Forensic Science International*, *286*, 245–251. https://doi.org/10.1016/j.forsciint.2018.03.026

Honsberger, H., Werner, D., Rhumorbarbe, D., Riva, F., Glardon, M., Gallusser, A., & Delémont, O. (2019). How to recognise the traces left on a crime scene by a 3D-printed Liberator? Part 2. Elements of ammunition, marks on the weapons and polymer fragments. *Forensic Science International*, *295*, 137–144. https://doi.org/10.1016/j.forsciint.2018.12.010

Mattijssen, E. J. A. T., Kerkhoff, W., Hermsen, R., & Hes, R. A. G. (2023). Interpol review of forensic firearm examination 2019–2022. *Forensic Science International: Synergy*, *6*, 100305. https://doi.org/10.1016/j.fsisyn.2022.100305

AFTE. (1992). AFTE criteria for identification committee final report. *AFTE Journal, 24(3), 336-340. https://afte.org/store/product/afte-journal-vol-24-no-3-1992*

Duez, P., Weller, T., Brubaker, M., Hockensmith, R. E., & Lilien, R. (2018). Development and Validation of a Virtual Examination Tool for Firearm Forensics. *Journal of Forensic Sciences*, *63*(4), 1069–1084. https://doi.org/10.1111/1556-4029.13668

Weller, T., Brubaker, M., Duez, P., & Lilien, R. (2015). *Introduction and Initial Evaluation of a Novel Three-Dimensional Imaging and Analysis System for Firearm Forensics*. *47*(4).

Chapnick, C., Weller, T. J., Duez, P., Meschke, E., Marshall, J., & Lilien, R. (2020). Results of the 3D Virtual Comparison Microscopy Error Rate (VCMER) Study for firearm forensics. *Journal of Forensic Sciences*, *66*(2), 557–570. https://doi.org/10.1111/1556-4029.14602

Knowles, L., Hockey, D., & Marshall, J. (2022). The validation of 3D virtual comparison microscopy (VCM) in the comparison of expended cartridge cases. *Journal of Forensic Sciences*, *67*(2), 516–523. https://doi.org/10.1111/1556-4029.14942

Autodesk (2024). Autodesk Fusion 360. https://www.autodesk.com/products/fusion-360/personal

Prusa Research (2024). PrusaSlicer 2.7.4. https://www.prusa3d.com/en/page/prusaslicer_424/

Fawcett, T. (2006). An introduction to ROC analysis. *Pattern Recognition Letters*, *27*(8), 861–874. https://doi.org/10.1016/j.patrec.2005.10.010

Kulkarni, A., Chong, D., & Batarseh, F. A. (2020). Foundations of data imbalance and solutions for a data democracy. In Data Democracy (pp. 83–106). Elsevier. https://doi.org/10.1016/B978-0-12-818366-3.00005-8

Narkhede, S. (2021, June 15). Understanding confusion matrix. Medium. https://towardsdatascience.com/understanding-confusion-matrix-a9ad42dcfd62

Appendix A: ROC Curves for Each Print Bed Surface

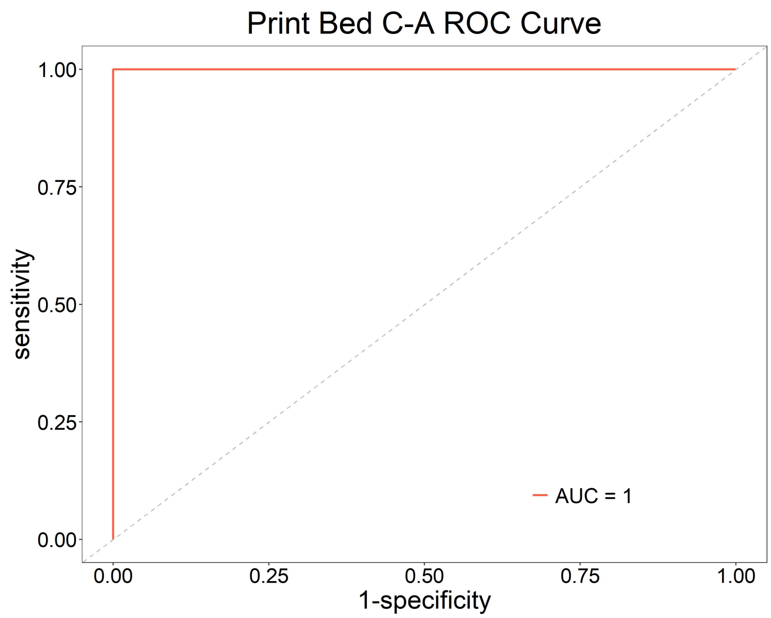

Figure 29. A ROC curve and AUC score generated for print bed surface C-A.

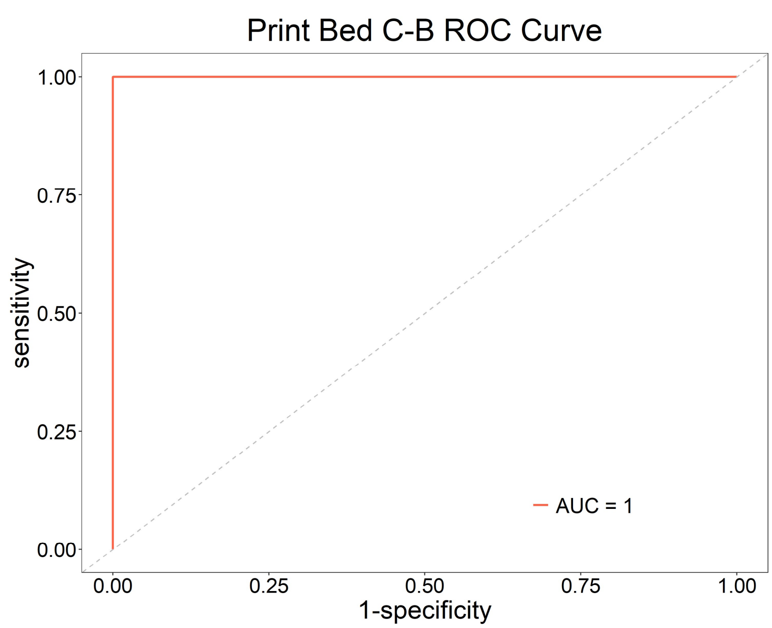

Figure 30. A ROC curve and AUC score generated for print bed surface C-B.

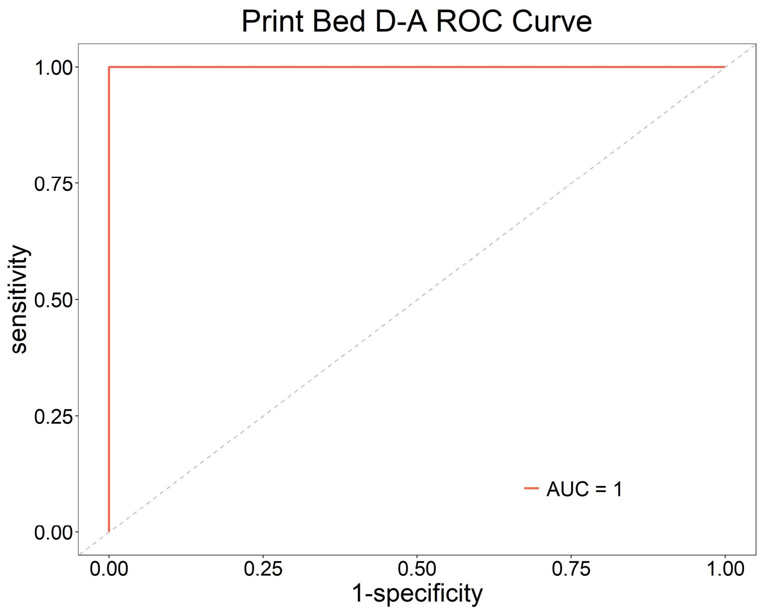

Figure 31. A ROC curve and AUC score generated for print bed surface D-A.

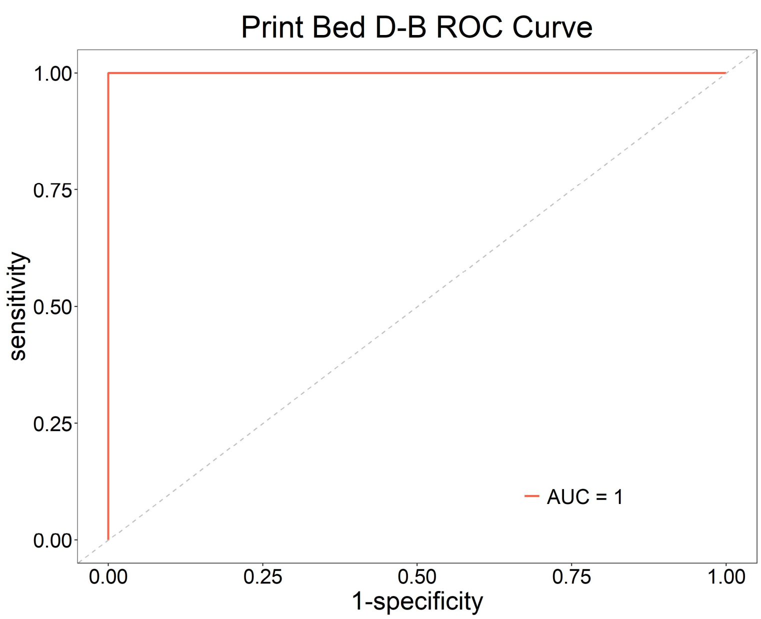

Figure 32. A ROC curve and AUC score generated for print bed surface D-B.

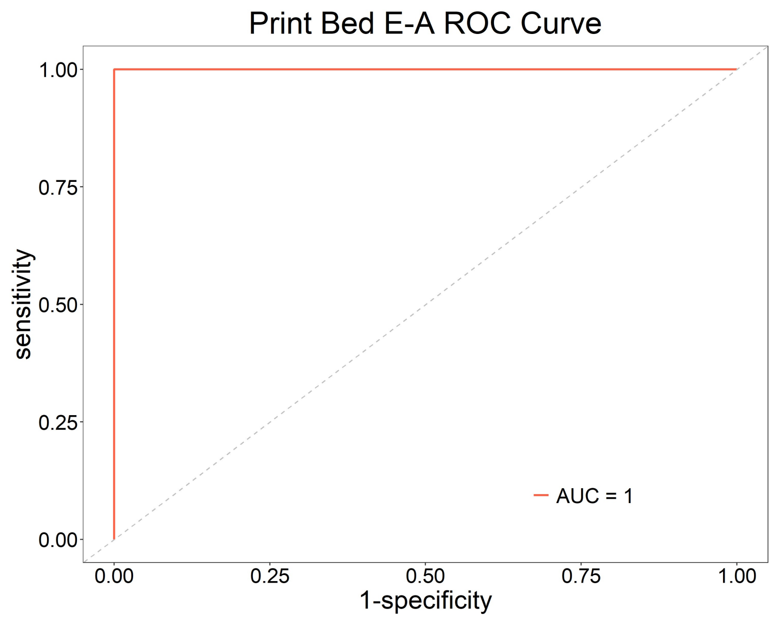

Figure 33. A ROC curve and AUC score generated for print bed surface E-A.

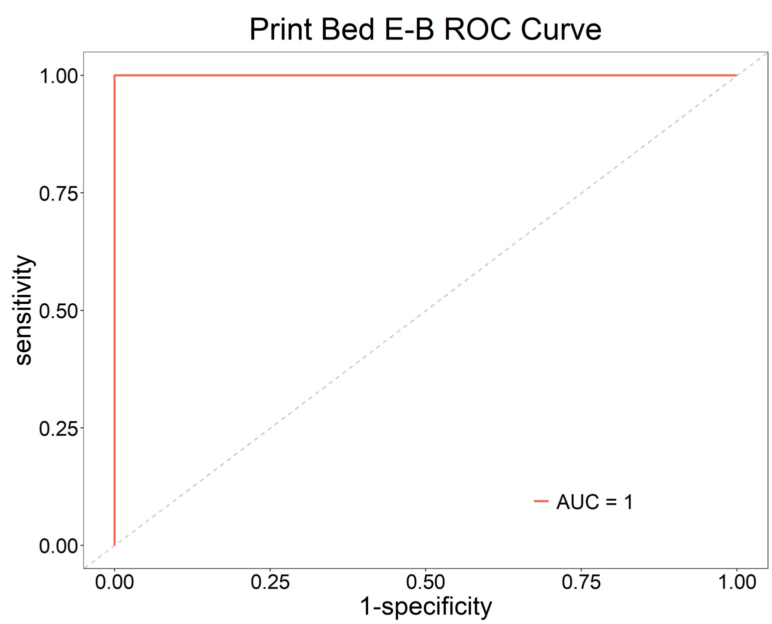

Figure 34. A ROC curve and AUC score generated for print bed surface E-B.

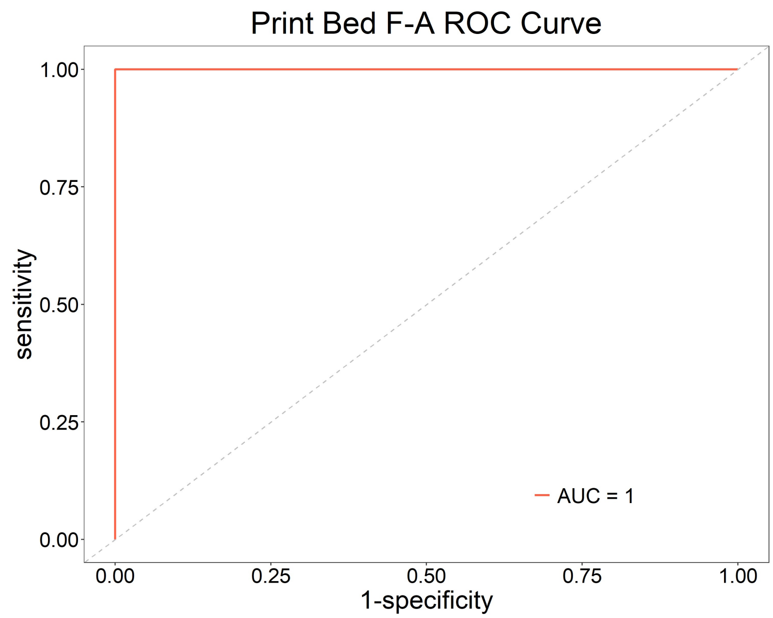

Figure 35. A ROC curve and AUC score generated for print bed surface F-A.

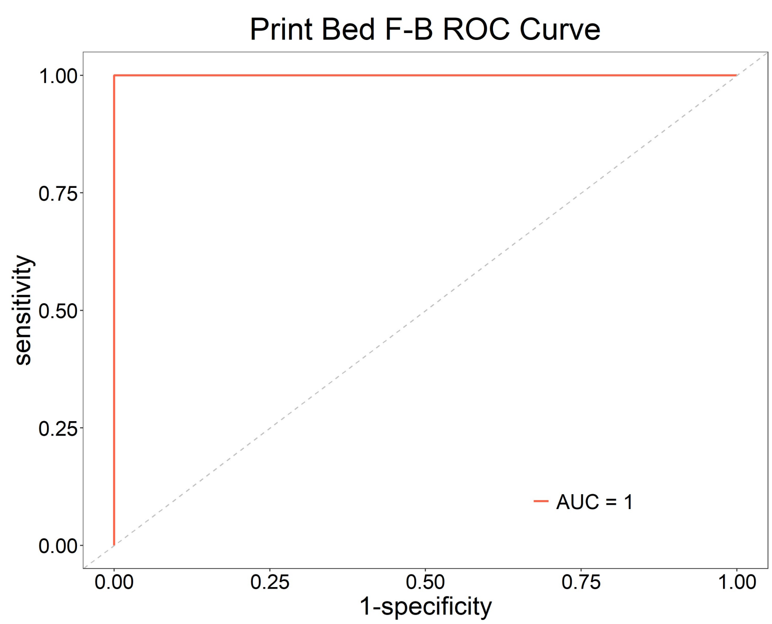

Figure 36. A ROC curve and AUC score generated for print bed surface F-B.

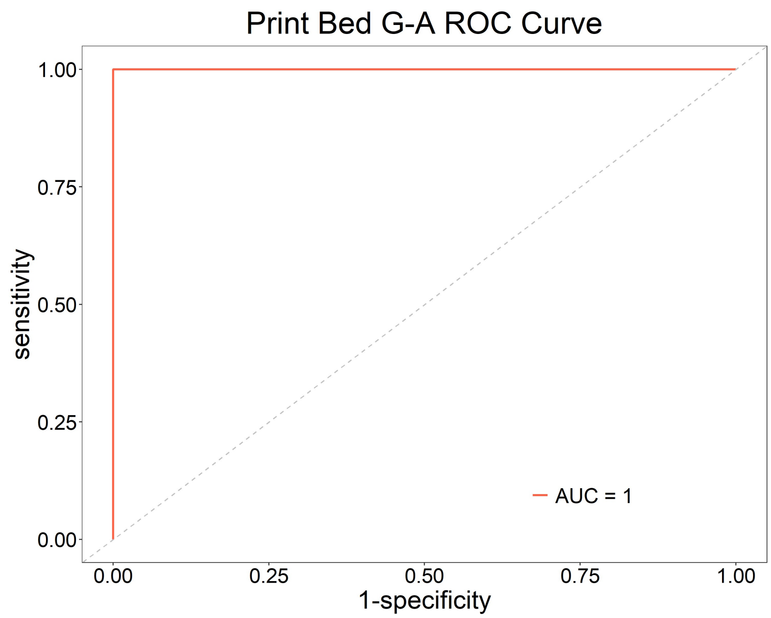

Figure 37. A ROC curve and AUC score generated for print bed surface G-A.

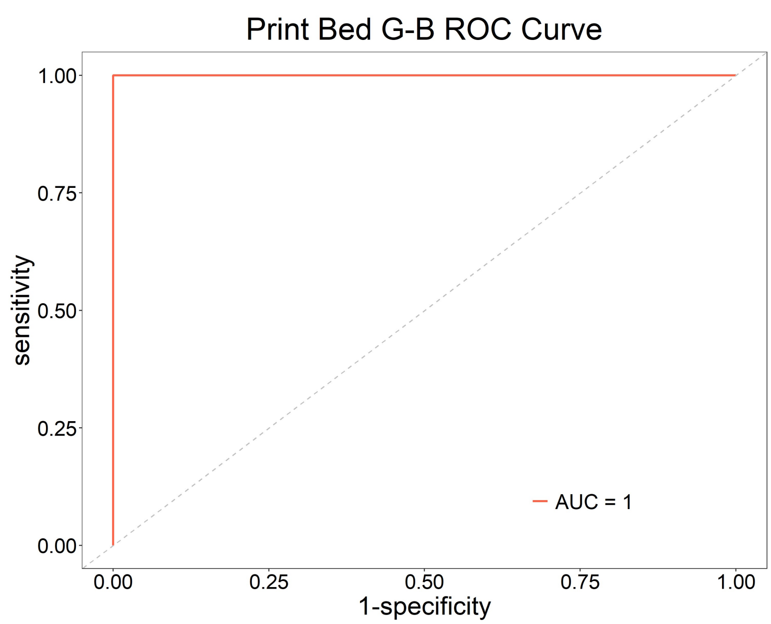

Figure 38. A ROC curve and AUC score generated for print bed surface G-B.

Appendix B: ROC Curves for Each Nozzle Surface

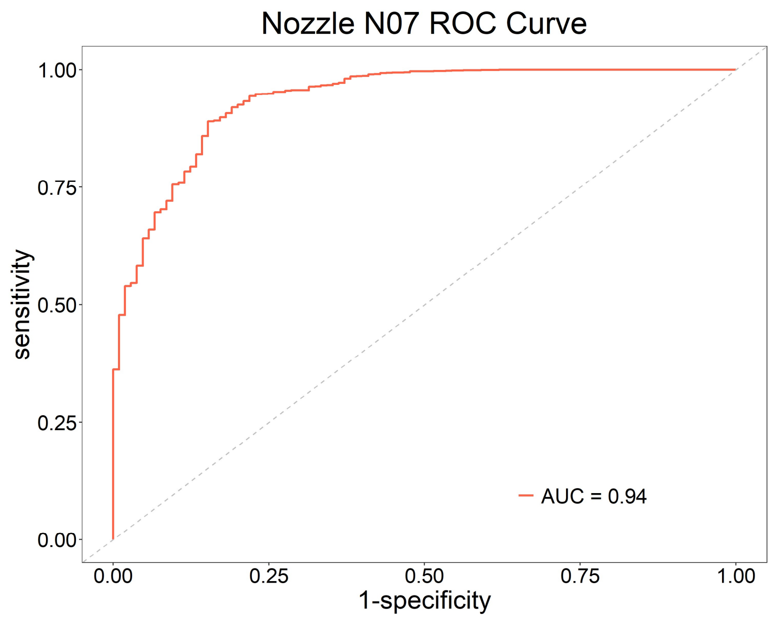

Figure 39. A ROC curve and AUC score generated for nozzle N07.

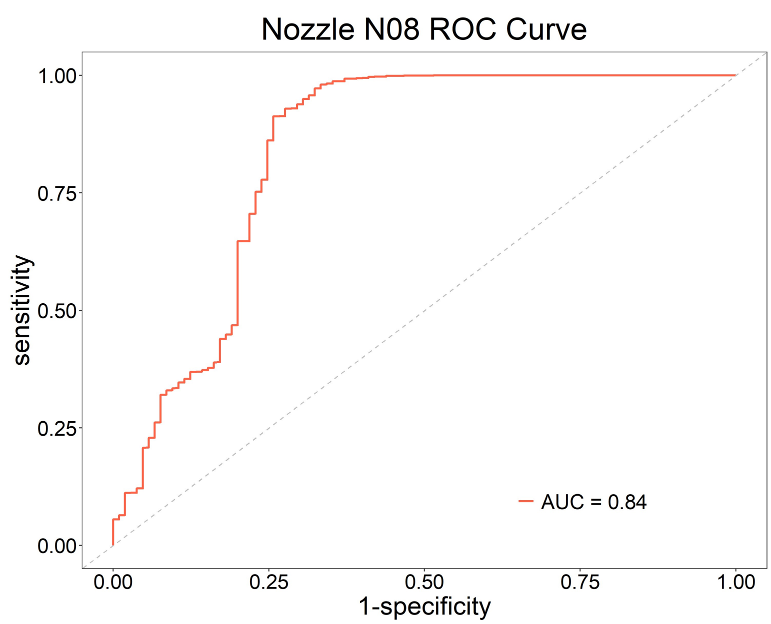

Figure 40. A ROC curve and AUC score generated for nozzle N08.

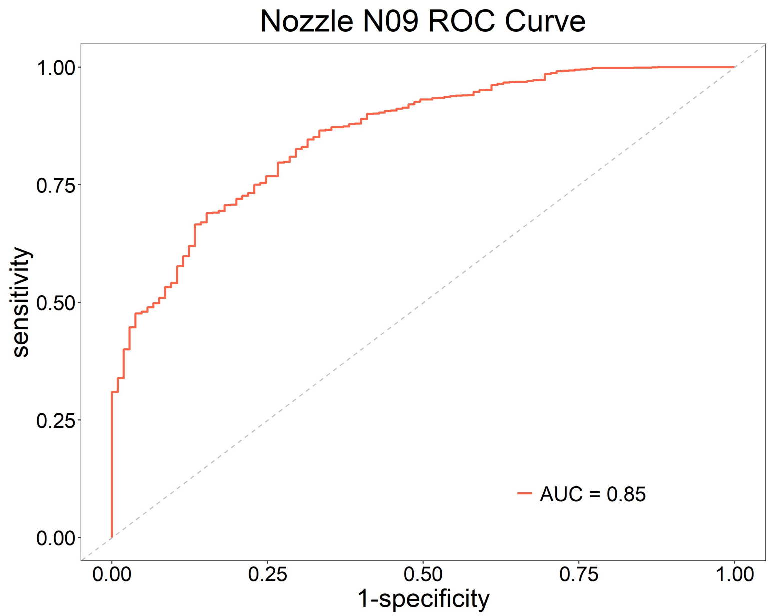

Figure 41. A ROC curve and AUC score generated for nozzle N09.

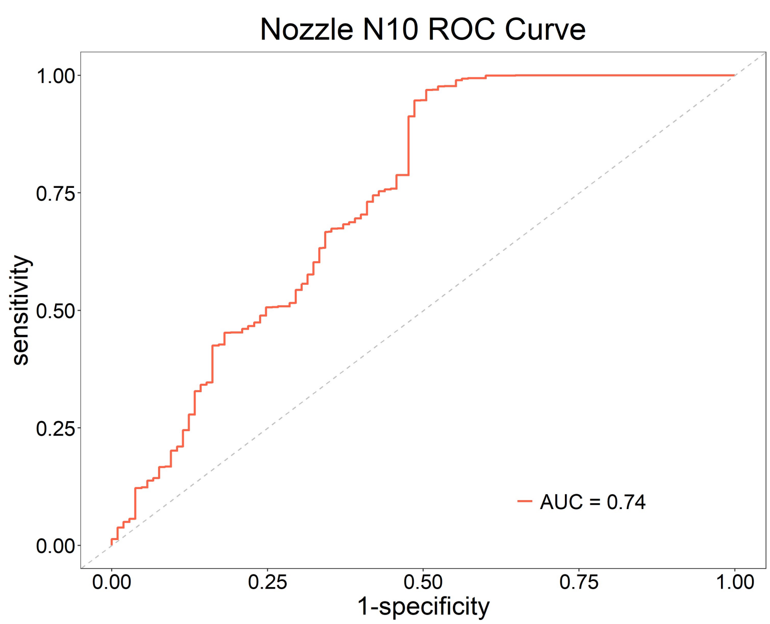

Figure 42. A ROC curve and AUC score generated for nozzle N10.

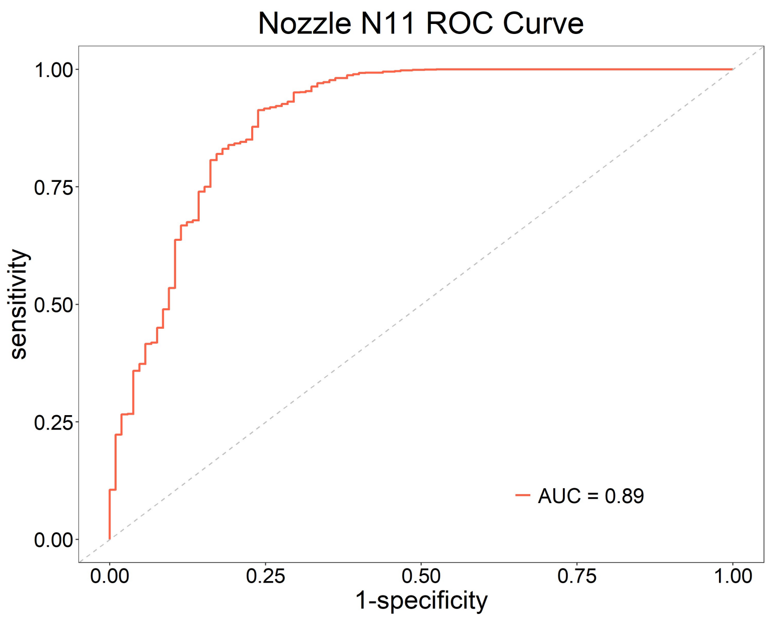

Figure 43. A ROC curve and AUC score generated for nozzle N11.

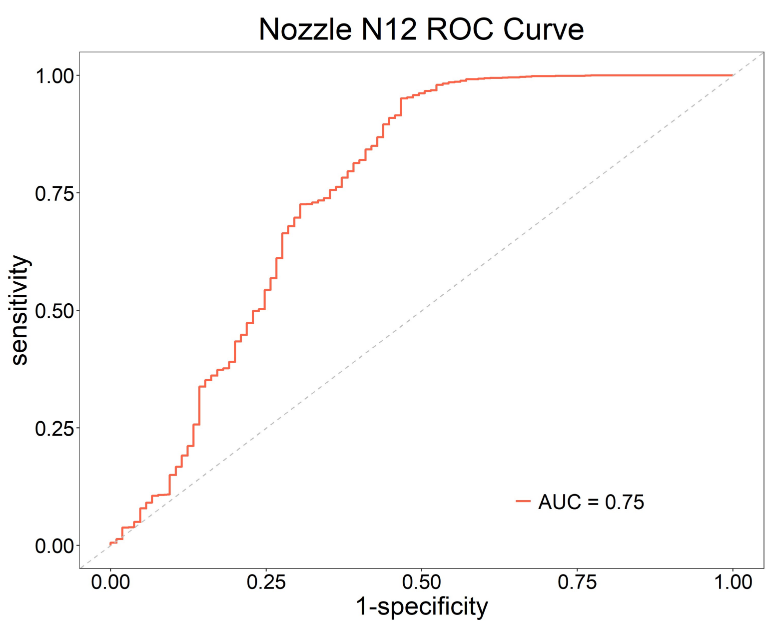

Figure 44. A ROC curve and AUC score generated for nozzle N12.

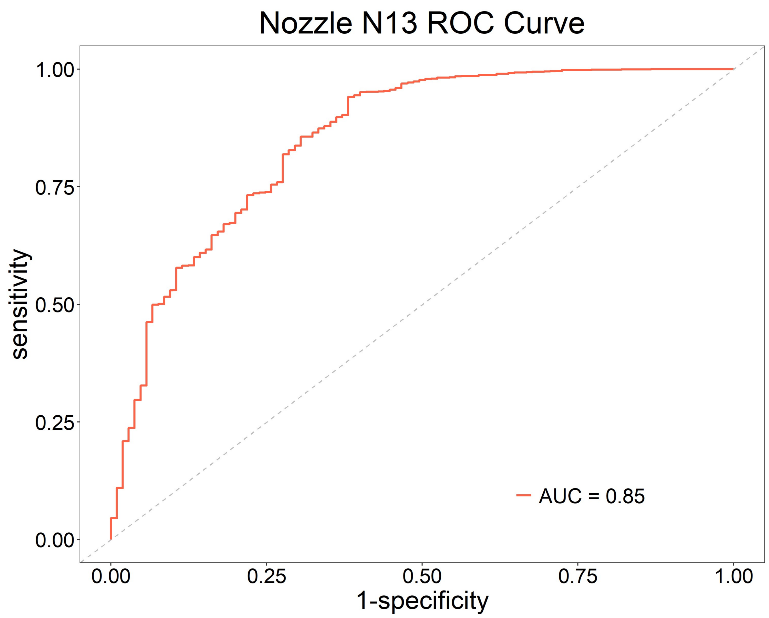

Figure 45. A ROC curve and AUC score generated for nozzle N13.

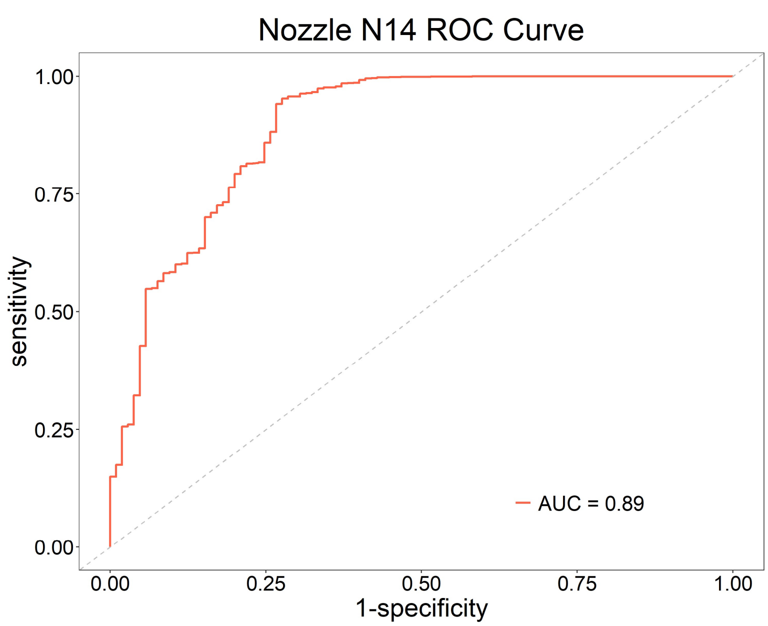

Figure 46. A ROC curve and AUC score generated for nozzle N14.

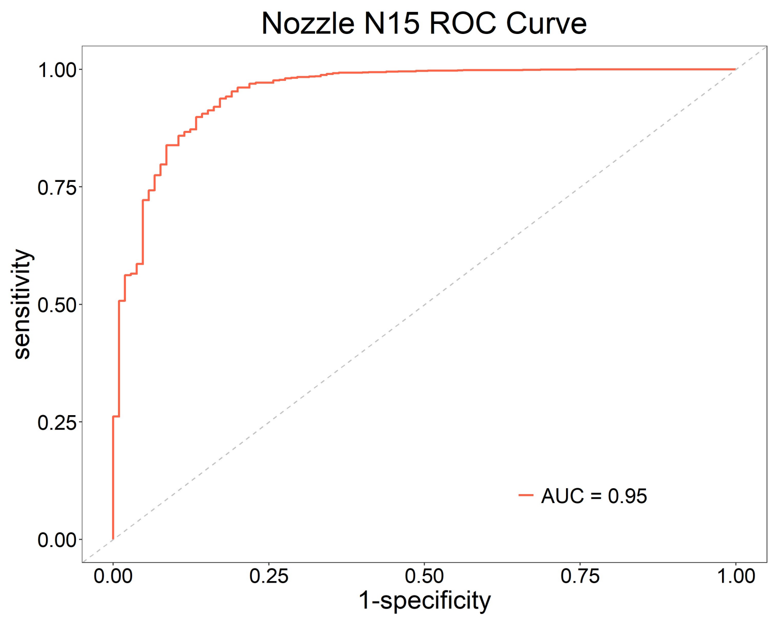

Figure 47. A ROC curve and AUC score generated for nozzle N15.

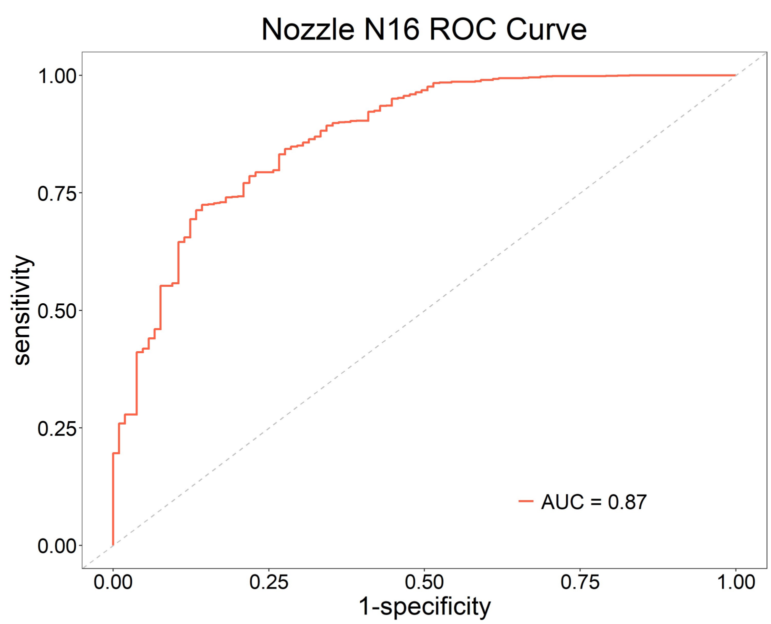

Figure 48. A ROC curve and AUC score generated for nozzle N16.